ORIGINAL PAPER

P. Amado Mendes · A. Tadeu

Wave propagation in the presence of empty cracks in an elastic medium

Abstract This paper proposes the use of a traction boundary element method (TBEM) to evaluate 3D wave propagation in unbounded elastic media containing cracks whose geometry does not change along one direction. The proposed formulation is developed in the frequency domain and handles the thin-body difficulty presented by the classical boundary element method (BEM). The empty crack may have any geometry and orientation and may even exhibit null thickness. Implementing this model yields hypersingular integrals, which are evaluated here analytically, thereby surmounting one of the drawbacks of this formulation. The TBEM formulation enables the crack to be modelled as a single line, allowing the computation of displacement jumps in the opposing sides of the crack. Furthermore, if this formulation is combined with the classical BEM formulation the displacements in the opposing sides of the crack can be computed by modelling the crack as a closed empty thin body.

1 Introduction

The modeling and analysis of scattered wave fields produced by rigid or elastic inclusions, cavities and cracks have been researched in several disciplines related to the remote detection, location and identification of defects (for instance, non-destructive evaluation and seismic prospection). In many industrial fields, such as the aerospace, automotive, structures and building components industries, numerical analysis and computational simulations have increasingly been replacing

full-scale and prototype laboratory testing. This has been happening both in the conception and design of new elements and also in the maintenance of structures during their lifetime.

The finite element method (FEM) and the boundary element method (BEM) are among the numerical techniques most often employed to perform these analyses. One major attractive feature of the BEM is that only the domain interfaces need to be discretized into elements. This corresponds to reducing (by one) the problem's dimension, since in two-dimensional (2D) problems only the line boundary of the domain is discretized and in three-dimensional (3D) problems only the surface of the domain needs to be discretized. Other advantages of the BEM include the automatic verification of the far-field conditions in unbounded or layered media, the way it can easily handle irregular geometries and the precision achieved, without the discretization of the interior domains [3, 34, 40].

Over the last 30 years, and in the context of linear elastic fracture mechanics, the BEM has proved to be one of the most efficient and accurate numerical tools for estimating stress intensity factors and analyzing crack growth problems. But it has also been applied to other problems in the field of fracture mechanics, like nonlinear and time dependent problems, as reviewed in Aliabadi [1]. However, using the BEM in problems involving very thin bodies or cracks leads to singularities in the matrix system of equations, and thence to mathematical degenerations in the numerical formulation [10]. Therefore, one of the main boundary element formulations adopted for the analysis of crack problems is referred to as the dual boundary element method (DBEM). In this method, a single region formulation is achieved with the displacement boundary integral equation discretizing one of the crack surfaces, while the traction boundary integral equation is used to discretize the opposite crack surface [2, 10]. The proposed formulation can be used for arbitrary geometry cracks subjected to any type of loading. Various examples can be found in Aliabadi [2] to demonstrate the capability and robustness of the dual boundary element methods in different fracture mechanics' fields. Such fields include elastostatics (with the evaluation of the stress intensity factor and crack

P. Amado Mendes · A. Tadeu (✉)
Department of Civil Engineering, University of Coimbra
Pólo II – Pinhal de Marrocos, 3030-290 Coimbra
Portugal
E-mail: tadeu@dec.uc.pt
Tel.: +351 239 797204
Fax: +351 239 797190

growth analysis), dynamic fracture mechanics, thermoelastic problems (in steady and transient states and fatigue problems), elastoplastics and cracks in anisotropic and composite materials.

In the case of dynamic fracture mechanics problems, when stationary cracks are subjected to dynamic loads [20], time dependent (or dynamic) stress intensity factors are normally computed by three different approaches. These are based on the elastostatic solution: one that involves the discretization of both space and time variations and the use of time domain fundamental solutions for the displacement and traction equations, referred to as the time domain method [11, 14]. Another way is to use the Laplace and Fourier transforms of the displacement and traction integral equations, of the fundamental elastodynamics solutions, and of the displacements' and tractions' nodal values. The unknown displacements and tractions, as functions of time are then computed (by numerical inversion) from the unknown transformed variables, which are obtained for a series of Laplace or Fourier parameters [15, 25, 30, 31, 33]. The third alternative is the dual reciprocity method, where the equations of motion are expressed in a boundary integral form using the fundamental solutions of elastostatics [13, 23]. The time domain, Laplace transform and dual reciprocity methods have been compared in relation to computational efficiency (i.e. storage/memory needs, computing time requirements and accuracy attained) in Fedelinsk et al. [16].

When the classical boundary integral representation is differentiated and the collocation point is taken to the boundary, the hypersingular formulation of the BEM is obtained. This technique has been used to solve static and dynamic, potential and elasticity problems. Although the hypersingular boundary element (HBE) formulation have applications far beyond fracture mechanics problems, it is the crack related problems that typify the use of the HBE. When using this type of formulation, two main difficulties arise: the first is the continuity conditions that must be guaranteed by the density functions, and the second is the need to perform the integration of strongly singular and hypersingular kernels that come up after differentiating the classical ones. A number of approaches have been proposed to deal with both difficulties (among others, see [30] and [5]), in particular relating to the choice of the elements and collocation procedure to be used [10, 12, 21, 24, 32, 46] and concerning the implementation of regularization techniques or non-singular formulations [9, 12, 33, 42]. Other ways of dealing with the hypersingular integrals have been proposed in [19, 29] and [43], while in [25] and [26] an indirect approach to evaluate these integrals for the plane-strain cases in 2D problems has been adopted.

Also adopting the traction boundary integral equation to solve fracture mechanics and wave propagation related problems near bodies of small thickness, the traction boundary integral equation method (TBIEM) and the traction boundary element method (TBEM) have been proposed by different researchers [8, 25, 26, 30, 31, 41]. The TBEM has been applied to the 2D wave propagation analysis near flat

horizontal empty cracks with null thickness in elastic media in Prosper and Kausel [25] and Prosper [26].

The combination of the boundary integral equation for the displacements and its normal derivative along the boundary is also used to try to overcome the appearance of erroneous results at certain frequencies, when the conventional BEM models are applied to acoustic or elastic wave problems in the frequency domain [39]. The solutions at those frequencies, usually referred to as fictitious eigenfrequencies, may be spurious and they arise from the mathematical formulation of the conventional boundary integral equations [28]. To overcome this difficulty when solving dynamic soil-structure interaction problems with buried regions of finite extent, Pyl, Clouteau and Degrande [27] proposed a combination of the boundary integral equations for the displacement and its normal derivative along the boundary, making use of an imaginary coupling parameter. To avoid hypersingular terms arising in the resulting boundary integral equation, the authors replace the normal derivative with a finite difference approximation over a characteristic distance, still leading to an exact boundary integral equation. If that distance is small enough and the boundary is smooth, it is shown that fictitious eigenfrequencies are avoided and that the proposed formulation is unique.

Pyl, Clouteau and Degrande [27] modified a method previously proposed in Burton and Miller [6] for acoustic problems. They propose a linear combination of the original boundary integral equation for the pressure and its normal derivative, also known as the hypersingular boundary integral equation [28]. Both integral equations present a non-unique solution at frequencies that match the eigenfrequencies of an interior Dirichlet or Neumann problem. As long as the parameter that links the boundary integral equations has at least a small non-zero imaginary part, a unique solution is obtained and the difficulty of the fictitious eigenfrequencies is overcome. However, in the field of elastodynamics, the method presented in [6] leads to strongly singular kernels in the boundary integral equation for the traction. The use of regularization techniques to reduce the integrals' order of singularity near the point of singularity has been described in several published works [7, 44, 45]. Most of these techniques are related to fundamental solutions to the Laplace equations [28].

The present work computes the 3D wave field generated in an infinite elastic medium, containing an empty crack or thin cavity inclusion whose geometry remains constant along one direction (the z direction). The problems are formulated in the frequency domain using two different boundary element approaches. When the thickness of the cavity is null (crack) the TBEM is used. For thin cavities exhibitng some thickness, a mixed formulation involving both the TBEM and the BEM is developed. Notice that this mixed scheme can also be used to model a crack, requiring the discretization of both the upper and lower surfaces.

As the medium is 2D (its geometry is kept constant along the z direction) and the dynamic source 3D (such as a point load), this is often known as a two-and-a-half-dimensional, or
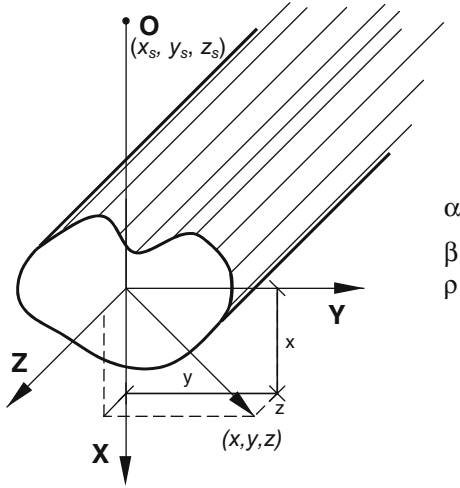
Fig. 1 Diagram of the problem geometry

$2\frac{1}{2}$D, problem, and the solution becomes much simpler. Solutions for such problems involve a spatial Fourier transform in the direction in which the geometry does not vary. A sequence of 2D problems with different spatial wavenumbers, k_z, must first be solved, and then the inverse Fourier transform is used to synthesize the 3D field. It should be noted that the final simplified equations obtained when $k_z = 0$ correspond to the pure 2D case.

In the next sections, the $2\frac{1}{2}$D problem is formulated and the boundary element formulations (BEM, TBEM and TBEM + BEM) are described. After the implementation of the proposed models, the solutions are verified against analytical solutions known for the case of a cylindrical circular empty cavity. A brief section describes how responses in the time domain are obtained by means of the fast Fourier transformation, using a Ricker pulse as the excitation dynamic wavelet source. The final part of the paper comprises a set of numerical results for 3D problems. Both frequency and time solutions are presented.

2 Problem formulation

Consider an empty cavity of infinite extension, with cylindrical geometry aligned along the z axis, as in Fig. 1. This inclusion is buried in an unbounded spatially uniform medium, and is excited by a harmonic dilatational point source. The 3D source, placed at (x_s, y_s, z_s) in the elastic host medium, oscillates with angular frequency ω. The emitted field is given by a dilatational potential ϕ,

$$\phi_{inc} = \frac{Ae^{i\frac{\omega}{\alpha}\left(\alpha t - \sqrt{(x-x_s)^2+(y-y_s)^2+(z-z_s)^2}\right)}}{\sqrt{(x-x_s)^2+(y-y_s)^2+(z-z_s)^2}}, \quad (1)$$

with the subscript inc representing the incident field, A the wave amplitude, α the dilatational wave velocity permitted by the elastic medium, and $i = \sqrt{-1}$.

Since the geometry of the stated problem does not vary along the longitudinal z direction, the 3D incident field can

be formulated as a summation of 2D solutions after applying a Fourier transformation along that direction. These 2D problems correspond to different axial wavenumbers defined by

$$k_\alpha = \sqrt{\frac{\omega^2}{\alpha^2} - k_{zm}^2}, \quad (2)$$

with $Im(k_\alpha) < 0$, k_{zm} the axial (longitudinal) wavenumbers given by $k_{zm} = \frac{2\pi}{L_{vs}}m$, $(m = 0, 1, ..., M)$, and L_{vs} being the spatial interval between virtual point sources.

If those virtual sources are equally spaced along the z direction, and displaced in such a way as to prevent spatial contamination between them, that summation becomes discrete [4] and the incident field can be written as:

$$\hat{\phi}_{inc}(\omega, x, y, k_z) = \frac{-iA}{2}H_0\left(k_\alpha\sqrt{(x-x_s)^2+(y-y_s)^2}\right), \quad (3)$$

in which $H_n(...)$ are second Hankel functions of order n.

The pure 2D problem can be solved taking $k_z = 0$.

3 Boundary integral formulations

Three different boundary integral formulations are presented to solve the wave scattering in elastic media. One is the classical BEM, which enables the computation of wave propagation in the vicinity of inclusions which are not thin. The TBEM overcomes the thin-body difficulty, accounting for the presence of cracks without thickness. Finally, a combination of the BEM and TBEM formulations simulates the propagation of waves through media containing thin empty cavities.

3.1 Boundary element formulation (BEM)

Consider an empty cavity bounded by a surface, S, embedded in a homogeneous elastic medium of infinite extent and excited by spatially sinusoidal harmonic line loads with wavenumber k_z placed at x_s. Applying the reciprocity theorem, the boundary integral equation can be formulated and given by:

$$c_{ij}u_i(x_0, \omega) = -\int_S u_j(x, \omega) H_{ij}(x, n_n, x_0, \omega) ds$$
$$+u_i^{inc}(x_s, x_0, \omega). \quad (4)$$

In this equation, $i, j = 1, 2$ represent the normal and tangential directions relative to the inclusion's surface, respectively, while $i, j = 3$ represent the z direction. $H_{ij}(x, n_n, x_0, \omega)$ defines the tractions in direction j at x (on the boundary S), due to a unit point force in the direction i at x_0 (a collocation point). $u_j(x, \omega)$ corresponds to displacements in direction j at x, and $u_i^{inc}(x_s, x_0, \omega)$ to the displacement incident field at x_0 along direction i. The coefficient c_{ij} is equal to $\delta_{ij}/2$, with δ_{ij} being the Kronecker delta, when the boundary is smooth. The vector $n_n = (\cos\theta_n, \sin\theta_n)$ defines the unit outward normal relative to the boundary at x.

The Green's functions for displacements in the x, y and z directions in the host medium (namely $G_{rt}(\boldsymbol{x}, \boldsymbol{x}_0, \omega)$ with r, $t = x$, y, z, where r is the direction of the load and t the direction of the displacement), are derived at Tadeu and Kausel [38]. The tractions along the x, y and z directions, in the same solid medium, are obtained by derivatives of these Green's functions:

$$
\begin{aligned}
H_{rx} = 2\mu &\left[\frac{\alpha^2}{2\beta^2} \frac{\partial G_{rx}}{\partial x} + \left(\frac{\alpha^2}{2\beta^2} - 1 \right) \right.\\
&\left. \times \left(\frac{\partial G_{ry}}{\partial y} + \frac{\partial G_{rz}}{\partial z} \right) \right] \cos\theta_n \\
+\mu &\left[\frac{\partial G_{ry}}{\partial x} + \frac{\partial G_{rx}}{\partial y} \right] \sin\theta_n \\
H_{ry} = 2\mu &\left[\left(\frac{\alpha^2}{2\beta^2} - 1 \right) \left(\frac{\partial G_{rx}}{\partial x} + \frac{\partial G_{rz}}{\partial z} \right) \right.\\
&\left. +\frac{\alpha^2}{2\beta^2} \frac{\partial G_{ry}}{\partial y} \right] \sin\theta_n \\
+\mu &\left[\frac{\partial G_{ry}}{\partial x} + \frac{\partial G_{rx}}{\partial y} \right] \cos\theta_n \\
H_{rz} = \mu &\left[\frac{\partial G_{rx}}{\partial z} + \frac{\partial G_{rz}}{\partial x} \right] \cos\theta_n \\
+\mu &\left[\frac{\partial G_{ry}}{\partial z} + \frac{\partial G_{rz}}{\partial y} \right] \sin\theta_n,
\end{aligned}
\tag{5}
$$

with $H_{rt} = H_{rt}(\boldsymbol{x}, n_n, \boldsymbol{x}_0, \omega)$ and $G_{rt} = G_{rt}(\boldsymbol{x}, \boldsymbol{x}_0, \omega)$. In order to obtain $H_{ij}(\boldsymbol{x}, n_n, \boldsymbol{x}_0, \omega)$ in the normal and tangential directions, these expressions can be combined. In these equations $\mu = \rho\,\beta^2$, with β being the shear wave velocity and ρ the density of the medium.

The solution of the boundary integral equation for a general cross section is obtained after discretizing both the boundary and boundary values. The application of a unitary virtual load to the different nodes along the boundary leads to a system of linear equations, where nodal tractions are related, which can be solved for the nodal displacements.

The integrations are evaluated numerically using a Gaussian quadrature scheme, when the element to be integrated is not the loaded element. When the element to be integrated is the loaded one, the integrations are performed in closed form, as in Tadeu et al. [36] and [37].

3.2 Traction boundary element formulation (TBEM)

When modeling the scattered wave field in the vicinity of thin empty cavities, the BEM formulation described above fails. The traction boundary element method (TBEM) can be proposed to handle that difficulty [25,26]. This formulation can be expressed by the following equation:

$$
\begin{aligned}
a\, u_i(\boldsymbol{x}_0, \omega) = &-\int_S u_j(\boldsymbol{x}, \omega)\; \bar{H}_{ij}(\boldsymbol{x}, n_n, \boldsymbol{x}_0, \omega)\;\mathrm{d}s \\
&+\bar{u}_i^{\text{inc}}(\boldsymbol{x}_s, \boldsymbol{x}_0, n_n, \omega).
\end{aligned}
\tag{6}
$$

This equation can be seen as the result of the application of dipoles (dynamic doublets). In the equation, i, $j = 1$, 2 correspond to the normal and tangential directions relative to the inclusion's surface, respectively, while i, $j = 3$ correspond to those in the z direction. The coefficient a is null for piecewise straight boundary elements, as stated in Guiggiani [17]. Applying the traction operator to $H_{ij}(\boldsymbol{x}, n_n, \boldsymbol{x}_0, \omega)$, the terms can be defined as $\bar{H}_{ij}(\boldsymbol{x}, n_n, \boldsymbol{x}_0, \omega)$, which can be taken as the combination of the derivatives of Eq. (4), in order to x, y and z, so as to obtain stresses $\bar{H}_{ij}(\boldsymbol{x}, n_n, \boldsymbol{x}_0, \omega)$. $n_n = (\cos\theta_n, \sin\theta_n)$ is defining the unit outward normal relative to the boundary element, at $\boldsymbol{x}$. Performing the equilibrium of stresses, the following equations can be written along x, y and z, caused by loads also applied along the same x, y and z directions:

$$
\begin{aligned}
\bar{H}_{xr} = 2\mu &\left[\frac{\alpha^2}{2\beta^2} \frac{\partial H_{xr}}{\partial x} + \left(\frac{\alpha^2}{2\beta^2} - 1 \right) \right.\\
&\left. \times \left(\frac{\partial H_{yr}}{\partial y} + \frac{\partial H_{zr}}{\partial z} \right) \right] \cos\theta_0 \\
+\mu &\left[\frac{\partial H_{yr}}{\partial x} + \frac{\partial H_{xr}}{\partial y} \right] \sin\theta_0 \\
\bar{H}_{yr} = 2\mu &\left[\left(\frac{\alpha^2}{2\beta^2} - 1 \right) \left(\frac{\partial H_{xr}}{\partial x} + \frac{\partial H_{zr}}{\partial z} \right) \right.\\
&\left. +\frac{\alpha^2}{2\beta^2} \frac{\partial H_{yr}}{\partial y} \right] \sin\theta_0 \\
+\mu &\left[\frac{\partial H_{yr}}{\partial x} + \frac{\partial H_{xr}}{\partial y} \right] \cos\theta_0 \\
\bar{H}_{zr} = \mu &\left[\frac{\partial H_{xr}}{\partial z} + \frac{\partial H_{zr}}{\partial x} \right] \cos\theta_0 \\
+\mu &\left[\frac{\partial H_{yr}}{\partial z} + \frac{\partial H_{zr}}{\partial y} \right] \sin\theta_0,
\end{aligned}
\tag{7}
$$

where $n_0 = (\cos\theta_0, \sin\theta_0)$ is defining the unit outward normal at $\boldsymbol{x}_0$ (the collocation point), and $\bar{H}_{tr} = \bar{H}_{tr}(\boldsymbol{x}, n_n, \boldsymbol{x}_0, \omega)$, $H_{tr} = H_{tr}(\boldsymbol{x}, n_n, \boldsymbol{x}_0, \omega)$ with r, $t = x$, y, z.

In a similar way to the evaluation of $\bar{H}_{tr}$, the incident field component in terms of stresses can be evaluated by:

$$
\begin{aligned}
\bar{u}_x^{\text{inc}} = 2\mu &\left[\frac{\alpha^2}{2\beta^2} \frac{\partial u_x^{\text{inc}}}{\partial x} + \left(\frac{\alpha^2}{2\beta^2} - 1 \right) \right.\\
&\left. \times \left(\frac{\partial u_y^{\text{inc}}}{\partial y} + \frac{\partial u_z^{\text{inc}}}{\partial z} \right) \right] \cos\theta_0 \\
+\mu &\left[\frac{\partial u_y^{\text{inc}}}{\partial x} + \frac{\partial u_x^{\text{inc}}}{\partial y} \right] \sin\theta_0 \\
\bar{u}_y^{\text{inc}} = 2\mu &\left[\left(\frac{\alpha^2}{2\beta^2} - 1 \right) \left(\frac{\partial u_x^{\text{inc}}}{\partial x} + \frac{\partial u_z^{\text{inc}}}{\partial z} \right) \right.\\
&\left. +\frac{\alpha^2}{2\beta^2} \frac{\partial u_y^{\text{inc}}}{\partial y} \right] \sin\theta_0
\end{aligned}
\tag{8}
$$

$$+\mu \left[\frac{\partial u_y^{\text{inc}}}{\partial x} + \frac{\partial u_x^{\text{inc}}}{\partial y} \right] \cos \ \theta_0$$

$$\bar{u}_z^{\text{inc}} = \mu \left[\frac{\partial u_x^{\text{inc}}}{\partial z} + \frac{\partial u_z^{\text{inc}}}{\partial x} \right] \cos \ \theta_0$$

$$+\mu \left[\frac{\partial u_y^{\text{inc}}}{\partial z} + \frac{\partial u_z^{\text{inc}}}{\partial y} \right] \sin \ \theta_0,$$

with $\bar{u}_r^{\text{inc}} = \bar{u}_r^{\text{inc}}(\mathbf{x}_s, \mathbf{x}_0, n_n, \omega)$, $u_r^{\text{inc}} = u_r^{\text{inc}}(\mathbf{x}_s, \mathbf{x}_0, \omega)$ and $r = x, \ y, \ z$.

The combination of these expressions can provide $\bar{H}_{ij}(\mathbf{x}, n_n, \mathbf{x}_0, \omega)$ and $\bar{u}_i^{\text{inc}}(\mathbf{x}_s, \mathbf{x}_0, n_n, \omega)$ in the normal and tangential directions.

The solution of the boundary integral Eq. (6) can be achieved by discretizing the boundary into N straight boundary elements, with one nodal point in the middle of each element. A set of integrations therefore needs to be calculated, and this is done by applying a Gaussian quadrature scheme, in the case of elements that do not coincide with the loaded elements. In the case of coincidence between those elements, hypersingular integrals arise and they are evaluated by the technique described below. The integrations are performed for a horizontal boundary element, since the system of equations can be written considering the normal, tangential and z directions relative to the boundary element. In this situation, the integrations along the loaded element are independent of its orientation and it can be taken that: $\cos \ \theta_n = \cos \ \theta_0 = 0$ and $\sin \ \theta_n = \sin \ \theta_0 = 1.0$.

3.2.1 Hypersingular integrations

An indirect approach is proposed for the analytical solution of those hypersingular integrals. This consists of defining the dynamic equilibrium of an isolated semi-cylinder defined above the boundary of each boundary element. Its derivation is presented in the Appendix.

3.3 TBEM + BEM formulation

The two formulations can be applied jointly, thereby solving these problems and the cases of thin empty cavities. While part of the boundary surface is loaded with monopole loads, the rest is loaded with dipoles. If the TBEM + BEM formulation is adopted, the thin heterogeneities are discretized by closed surfaces. And in the case of null-thickness cavities, those surfaces are defined by coincident lines, and displacements at the upper and lower parts of the empty inclusions can be evaluated separately.

4 Verification of the BEM algorithms

The proposed boundary element formulations are verified by comparing their numerical results with analytical solutions known for the case of a circular empty cylindrical cavity with

a radius of 0.05 m. This free inclusion is placed in a homogeneous elastic medium and is subjected to a point dilatational load. The scattered wave field generated in the unbounded elastic medium can be evaluated in a circular cylindrical coordinate system (r, θ, z) by the separation of variables method [22,35].

The host elastic medium permits a dilatational wave speed of 2696.5 m/s and a shear wave speed of 1451.7 m/s, and has a mass density of 2140 kg/m^3. The point harmonic load exciting this medium is located at source point O (0.0 m, -0.125 m) and a receiver is placed at R (0.0 m, -0.075 m), as illustrated in Fig. 2a.

Computations of the x-, y- and z- displacement components were performed in the frequency range from [2000 Hz, 64000 Hz], for a spatial wavenumber in the z direction of 25 rad/m. The displacements obtained by both the TBEM and TBEM + BEM formulations are compared with the analytical and the numerical results given by the BEM model (Figs. 2b–d). In the different boundary element computations, 550 boundary elements were adopted. Both the real and imaginary parts of the responses can be seen, with the analytical solutions represented by solid and dashed lines, respectively, while the marked points correspond to the different boundary element models. The analytical and the numerical results are in very good agreement. Also note the coincidence between the three boundary element formulations. As the plane defined by $x = 0$ m is a plane of symmetry, the x-component displacements are null in the line of receivers R.

5 Time responses

The results computed by the boundary element models are obtained in the frequency domain. The application of an inverse (Fast) Fourier transform is required to analyze solutions in the time domain. A Ricker pulse is used as the time variation of the excitation source since it is not very demanding computationally, as it decays rapidly in time and frequency and enables an easy interpretation of the time signals' evolution. The temporal variation of the Ricker pulse is given by:

$$u(\tau) = A(1 - 2\tau^2)e^{-\tau^2}, \tag{9}$$

with A representing the amplitude; $\tau = (t - t_s)/t_0$, t corresponds to the time, t_s to the time when the wavelet attains its highest value, and πt_0 to the characteristic (dominant) period of the Ricker wavelet.

Applying a Fourier transform to Eq. (9), leads to:

$$U(\omega) = A \left[2t_0\sqrt{\pi} \ e^{-i\omega t_s} \right] \Omega^2 e^{-\Omega^2}, \tag{10}$$

where $\Omega = \omega t_0/2$.

The computation of this Fourier transformation leads to the addition of a finite number of terms, having different frequencies and spatial wavenumbers in the z direction. This is equivalent to adding evenly spaced sources with spatial intervals of $L_{vs} = 2\pi/\Delta k_z$ and time intervals of $T = 2\pi/\Delta\omega$
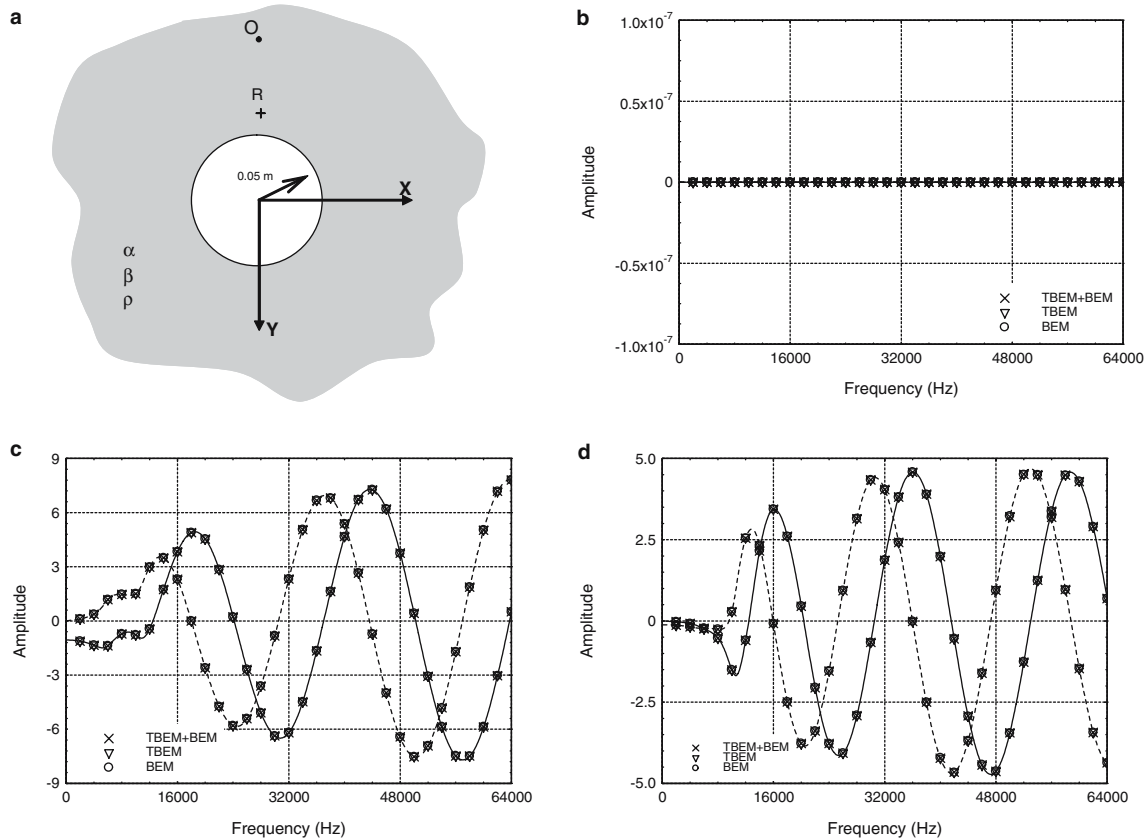
Fig. 2 BEM algorithms' verification against analytical solution: a) Diagram defining the circular cavity geometry, and source (O) and receiver (R) positions; b) $x-$component displacement; c) $y-$component displacement; d) $z-$component displacement

(with Δk_z and $\Delta \omega$ representing the wavenumber and the frequency increments, respectively). In order to avoid the aliasing phenomena and to reduce contamination of the response by adjacent virtual sources, complex frequencies with a small imaginary part of the form $\omega_c = \omega - i\eta$ (with $\eta = 0.7\Delta\omega$) are introduced. This procedure is later taken into account by rescaling the responses in the time domain with an exponential factor $e^{\eta t}$ [18].

6 Numerical applications

The wave propagation in the vicinity of an S-shaped empty crack is simulated by means of the boundary element formulations described and verified above. The geometry of the null-thickness cavity remains constant along the z direction ($2\frac{1}{2}$D problem) and is shown in Fig. 3 in a cross-sectional 2D view. The crack is located inside an unbounded elastic medium, which has a mass density of 2140 kg/m^3, a dilatational wave speed of 2696.5 m/s and a shear wave speed of 1451.7 m/s. This host medium is excited by a 3D harmonic point load located at point O (0.0 m, 0.0 m) on the vertical plane represented by $z = 0$ m.

First, the displacement jumps along that crack, obtained by the TBEM model, are compared with the displacements at the top and bottom of the same crack, given by the TBEM +

BEM model, for a specific frequency and spatial wavenumber. Afterwards, a set of 3D snapshots taken from computer animations at different time instants, makes the analysis of the TBEM time-dependent results easier. These examples illustrate the applicability of the present formulation to the wave propagation simulation around cracks, and this can be useful in the interpretation of non-destructive testing and seismic prospecting results.

6.1 Jumps of displacements

When the TBEM formulation is used, the S-shaped empty crack with null thickness is modelled as an open line (see Fig. 3). In this case, the jump of displacements between opposite surfaces of the crack, often referred to as the Crack Opening Displacement (COD), is evaluated directly at every nodal point of the surface being discretized on the vertical plane that contains the 3D source. On the other hand, if the TBEM + BEM formulation is adopted, the same null-thickness crack is discretized by a closed surface, with its upper part loaded by the TBEM and its lower part loaded by the BEM formulation. In this latter case, displacements are found at opposite/facing nodes on both surfaces of the crack.

The jump of displacements in the x, y and z directions, computed by the TBEM model at 16000 Hz when the free
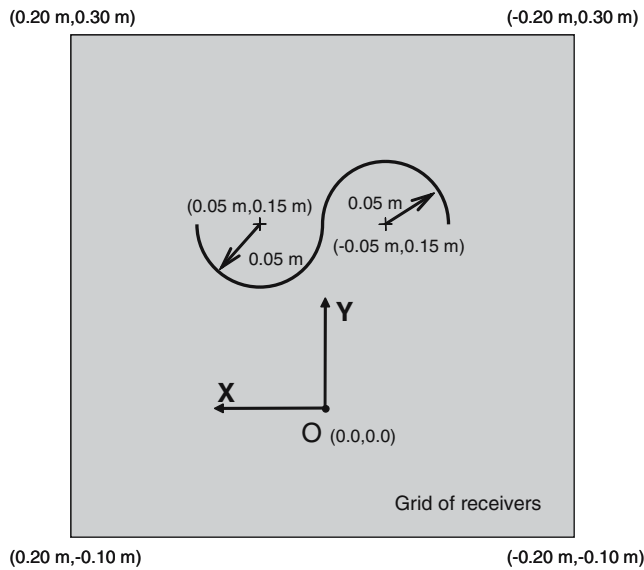
Fig. 3 2D view of S-shaped empty crack at xy plane

crack is excited by a dilatational point load with k_z=25 rad/m and discretized by an open line with 300 boudary elements, is presented in the first column of Fig. 4. The second and third columns of that Figure give, respectively, the displacements on the upper side and on the lower side of the crack (evaluated by the TBEM + BEM model, when the crack is discretized by coincident lines with a total number of 600 boundary elements), along the same directions. In those plots, the real and the imaginary parts of the response are presented as functions of the distance to the left extremity of the irregular crack. At every node of the discretized crack, the subtraction of the displacements from the upper and lower surfaces of the crack matches the displacement jumps (COD) given by the TBEM model. Also note that the responses are not symmetric with respect to the centre of the crack, owing to the irregularity of the geometry of the crack.

6.2 Synthetic time responses analysis

The time evolution of the scattered elastic wave field by the null-thickness S-shaped empty crack described previously, is simulated by the TBEM formulation. Fig. 3 shows the 2D geometry of the defined problem on the xy plane, which does not change along the z direction, and the positions of the 3D harmonic point source and receivers placed in the elastic unbounded medium. The null-thickness crack, embedded in that infinite elastic medium, is modelled as an open line and discretized using an appropriate number of boundary elements, defined by the relation between the wavelength (λ) and the length of the boundary elements (L), which is set to 8. The analysis of the time-dependent scattered wave field, evaluated by means of the TBEM formulation proposed above, is facilitated when complemented by the 3D computer animation snapshots.

Frequency results were computed in the range from 2000 Hz to 256000 Hz, with time responses obtained by applying an inverse (fast) Fourier transform in ω, using a Ricker pulse with a characteristic frequency of 75000 Hz for the source time evolution. A frequency increment of 2000 Hz specifies a total time window of 0.5 ms. The minimum number of boundary elements used for discretizing the crack was 300, at an initial frequency of 2000 Hz, and the maximum number of boundary elements used was 538, at the highest frequency of 256000 Hz.

Time results in terms of displacements along the x, y and z directions (u_x, u_y and u_z) were determined in fine grids of receivers placed in the unbounded medium over three orthogonal planes corresponding to: $x = -0.2$ m, $y = 0.3$ m and $z = 0.0$ m (Fig. 5). The grids of receivers were spaced at equal intervals, 0.004 m, along the x and y directions and 0.006 m in the longitudinal z direction.

The wave field propagation is characterized by 3D plots. These represent the summation of the direct incident wave field emitted by the point source with the scattering produced by the presence of the empty cavity in the unbounded medium at different time instants (Fig. 5). In these 3D snapshots of displacements u_x, u_y and u_z, a gray scale is used, in which the lighter and darker shades correspond respectively to higher and lower values of displacement amplitude.

The propagation of the incident pulses, diverging away from the source and spreading wave energy, can be observed at the initial time instants (see Fig. 5, at $t = 0.025$ ms). The x- and the y-components of the displacement field propagate symmetrically to the vertical and horizontal planes corresponding, respectively, to $x = 0.0$ m and $y = 0.0$ m. Along the vertical grid of receivers corresponding to $z = 0.0$ m there is no response for the z-displacement component, as that is the plane of the dilatational source and thus also a plane of symmetry. After striking the empty inclusion, which occurs at about $t = 0.041$ ms at the part nearest to point O in the convex part of the S-shaped crack, the waves are reflected back as P- and S-waves. This can be seen at $t = 0.070$ ms when it is still hard to distinguish the two types of waves because, in the initial stages, they overlap. For all displacement components, the time evolution of the incident pulses along the longitudinal direction start to be noted at this time on plane $x = -0.2$ m. At later time instants, P- and S-waves are clearly identifiable in all displacement fields at the orthogonal grids of receivers, as they travel away from the heterogeneity. Also visible for u_x and u_y, mainly at the vertical plane $z = 0.0$ m, are the wave energy trapped in the concave part of the crack facing the source point and the remaining energy being diffracted around the empty surface (see Fig. 5), at instants later than $t = 0.100$ ms. Largely due to the $2\frac{1}{2}$D geometry of the crack, a shadowed zone is formed in the side opposite the source, for all displacement components. This is most evident when the waves arrive at the upper grid of receivers (at plane $y = 0.3$ m, at times later than $t = 0.135$ ms). These later plots also show the 3D character of the wave propagation in the vicinity of this 2D crack.
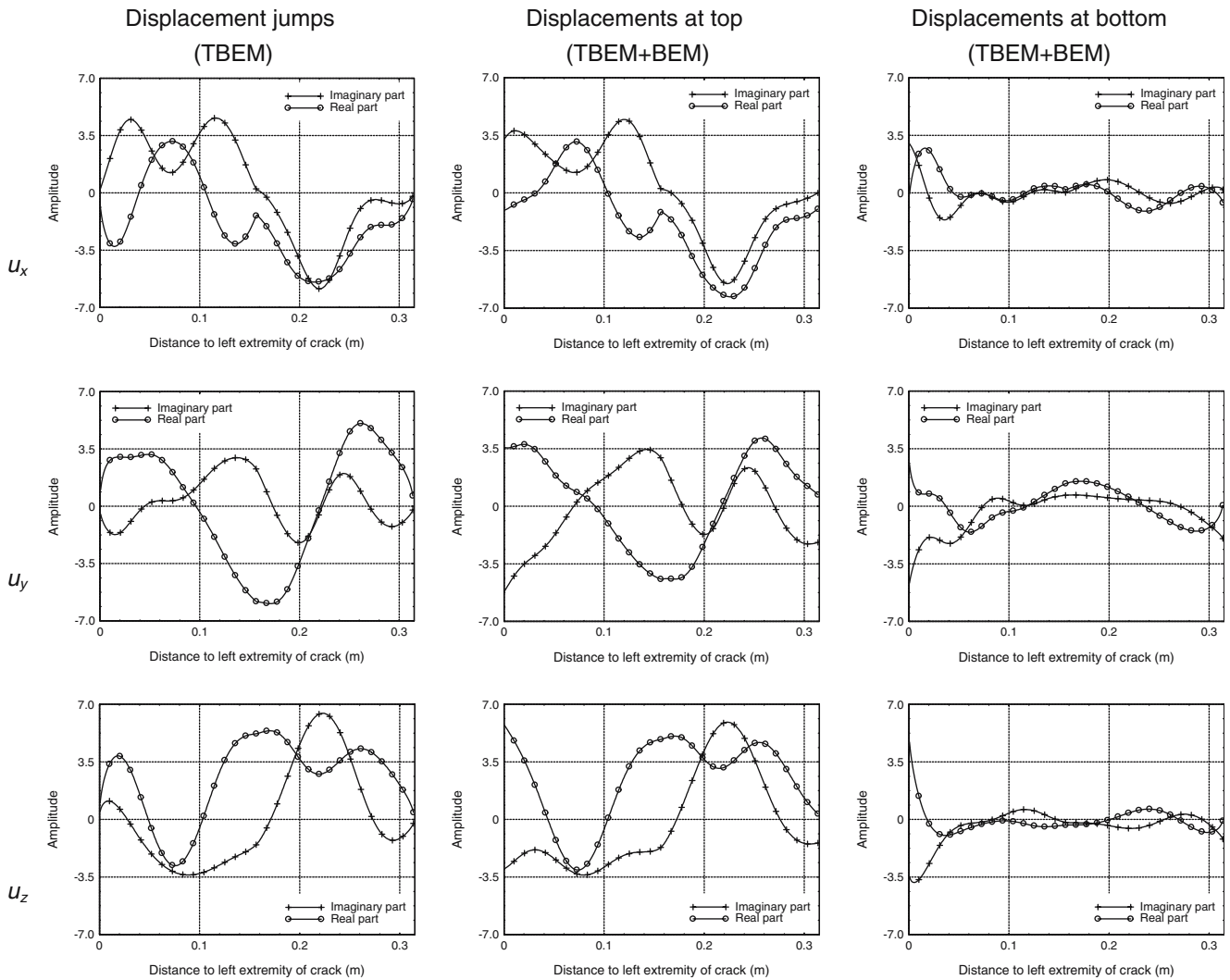
Fig. 4 Displacements at opposite sides of an S-shaped empty crack, at $f = 16000$ Hz. $x-$component, u_x, $y-$component, u_y, and $z-$component, u_z, displacements

7 Conclusions

The 3D wave field produced when a harmonic spherical source illuminates an empty irregular cylindrical crack (2D), which is submerged in an unbounded homogeneous elastic medium, has been calculated. The model is formulated in the frequency domain and, given the $2\frac{1}{2}$D geometry of the problem, it is expressed as a summation of waves with different spatial wavenumbers in the z direction. There is no limitation on the geometry and orientation of the crack.

Since the conventional direct BEM degenerates in the presence of thin bodies, two boundary element formulations based on the TBEM have been successfully proposed to address the wave propagation in the vicinity of thin or even null-thickness irregular heterogeneities. The TBEM has been adopted to discretize cracks with no thickness, and a mixed formulation that combines the TBEM and BEM is used to discretize thin heterogeneities. These formulations yield results that compare very well with analytical solutions and

with the classical BEM results for circular cylindrical empty inclusions. An indirect approach for the analytical evaluation of the hypersingular integrals that arise when solving the boundary integral equations in the TBEM and TBEM + BEM models is described.

The numerical examples analyzed show that the proposed formulations cope very well with the flat crack difficulty, for which the direct BEM fails. An S-shaped crack with null thickness was used to illustrate the applicability of the proposed TBEM formulation, for which displacement jumps and synthetic 3D time responses were computed.

Appendix – The analytical solution of hypersingular integrals

Considering a horizontal element, the normal, tangential and z directions correspond to the y, x and z directions, in that
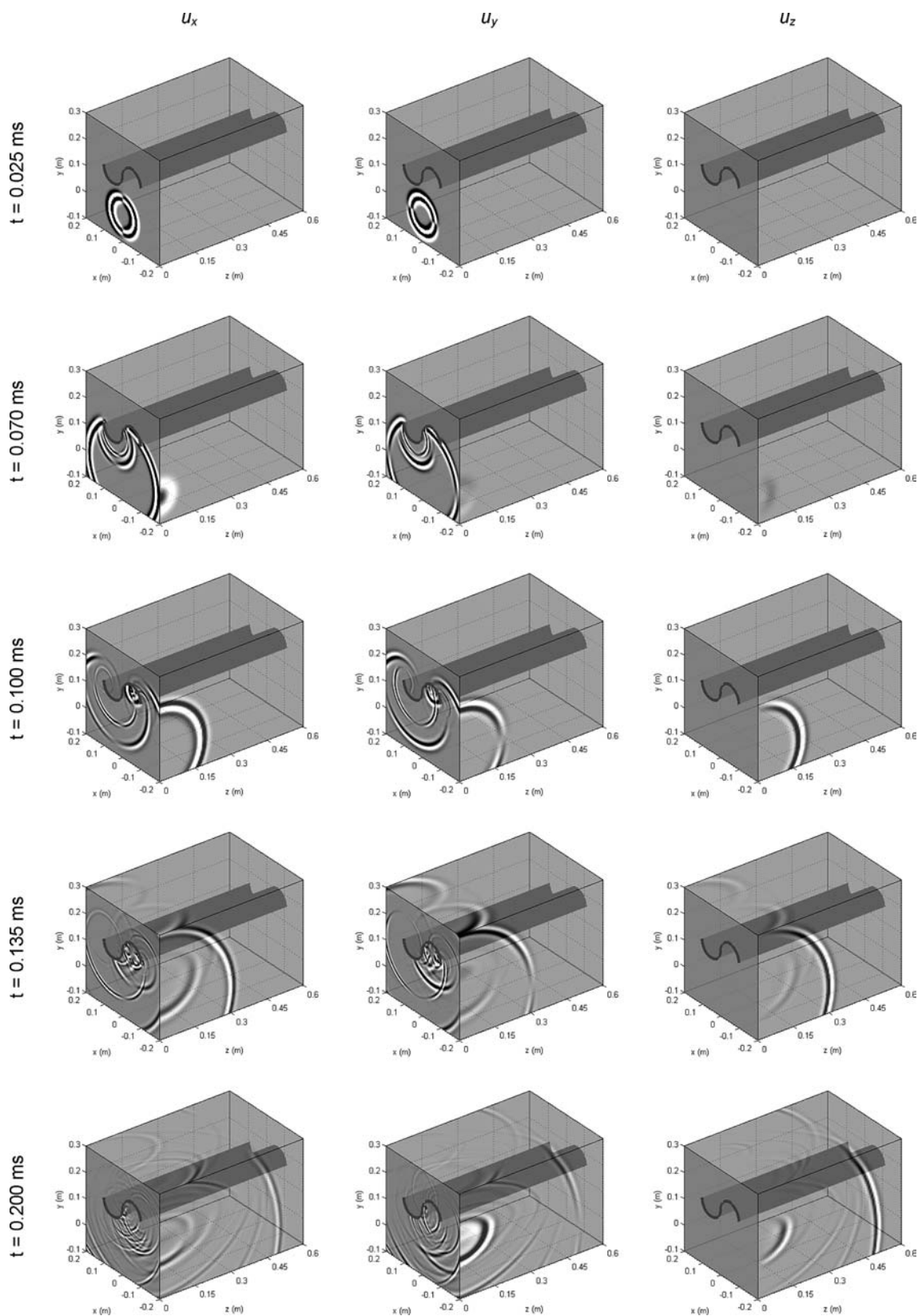
Fig. 5 Elastic scattering by an S-shaped empty crack in an unbounded medium. $x-$component, u_x, $y-$component, u_y, and $z-$component, u_z, displacements at different time instants

Fig. 6 Schematic diagram for performing the integration of $\frac{\partial H_{xx}}{\partial x}$, $\frac{\partial H_{xy}}{\partial x}$ and $\frac{\partial H_{xz}}{\partial x}$
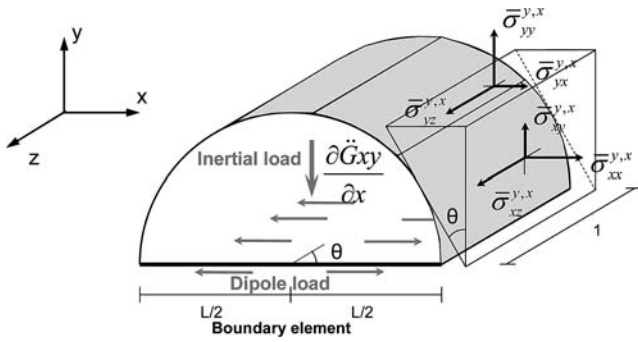

Fig. 7 Schematic diagram for performing the integration of $\frac{\partial H_{yx}}{\partial y}$, $\frac{\partial H_{yy}}{\partial y}$ and $\frac{\partial H_{yz}}{\partial y}$

Fig. 8 Schematic diagram for performing the integration of $\frac{\partial H_{zx}}{\partial z}$, $\frac{\partial H_{zy}}{\partial z}$ and $\frac{\partial H_{zz}}{\partial z}$

Fig. 9 Schematic diagram for performing the integration of $\frac{\partial H_{yx}}{\partial x}$, $\frac{\partial H_{yy}}{\partial x}$ and $\frac{\partial H_{yz}}{\partial x}$
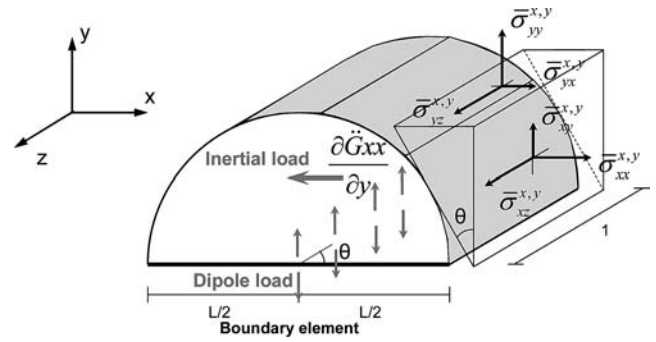

Fig. 10 Schematic diagram for performing the integration of $\frac{\partial H_{xx}}{\partial y}$, $\frac{\partial H_{xy}}{\partial y}$ and $\frac{\partial H_{xz}}{\partial y}$
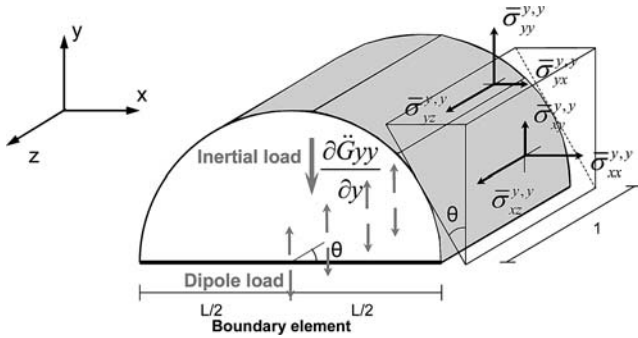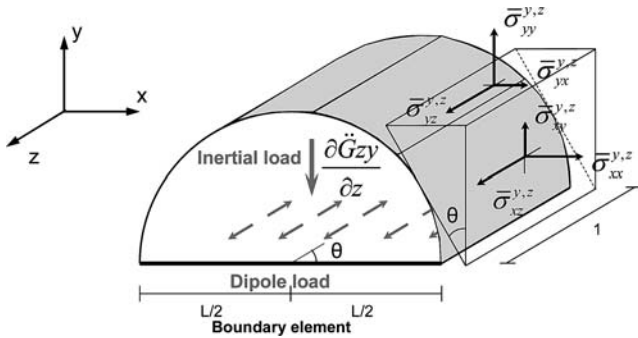
order. So, it follows from Eq. (7):

$$\overline{H}_{xr} = \mu \left[\frac{\partial H_{yr}}{\partial x} + \frac{\partial H_{xr}}{\partial y} \right] \tag{11}$$

$$\overline{H}_{yr} = 2\mu \left[\left(\frac{\alpha^2}{2\beta^2} - 1 \right) \left(\frac{\partial H_{xr}}{\partial x} + \frac{\partial H_{zr}}{\partial z} \right) \right.$$
$$\left. + \frac{\alpha^2}{2\beta^2} \frac{\partial H_{yr}}{\partial y} \right] \tag{12}$$

$$\overline{H}_{zr} = \mu \left[\frac{\partial H_{yr}}{\partial z} + \frac{\partial H_{zr}}{\partial y} \right]. \tag{13}$$

The hypersingular integrals that arise from the boundary integral Eq. (6) are evaluated by means of an indirect approach that represents the dynamic equilibrium of a semi-cylinder, detached immediately above the boundary element, as exemplified in Figs. 6–12.

1 Load along the normal direction

When the load is applied along the normal direction, the resultants along the horizontal, vertical and z directions arise from Eq. (12), according to:

$$\overline{H}_{yx} = 2\mu \left[\left(\frac{\alpha^2}{2\beta^2} - 1 \right) \left(\frac{\partial H_{xx}}{\partial x} + \frac{\partial H_{zx}}{\partial z} \right) \right.$$
$$\left. + \frac{\alpha^2}{2\beta^2} \frac{\partial H_{yx}}{\partial y} \right] \text{ (horizontal resultant)} \tag{14}$$

Fig. 11 Schematic diagram for performing the integration of $\frac{\partial H_{yx}}{\partial z}$, $\frac{\partial H_{yy}}{\partial z}$ and $\frac{\partial H_{yz}}{\partial z}$
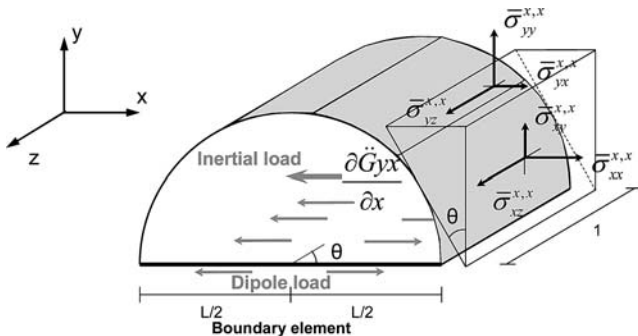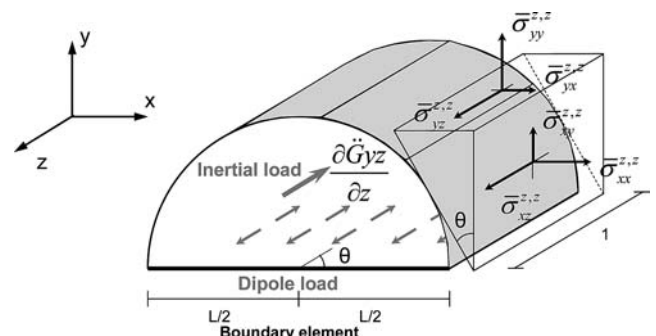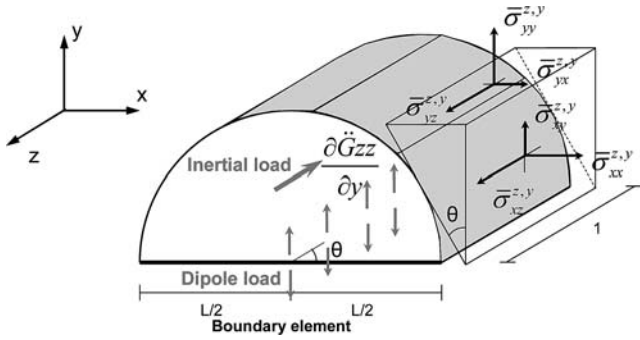
Fig. 12 Schematic diagram for performing the integration of $\frac{\partial H_{zx}}{\partial y}$, $\frac{\partial H_{zy}}{\partial y}$ and $\frac{\partial H_{zz}}{\partial y}$

$$\overline{H}_{yy} = 2\mu \left[\left(\frac{\alpha^2}{2\beta^2} - 1 \right) \left(\frac{\partial H_{xy}}{\partial x} + \frac{\partial H_{zy}}{\partial z} \right) \right.$$
$$\left. + \frac{\alpha^2}{2\beta^2} \frac{\partial H_{yy}}{\partial y} \right] \text{(vertical resultant)} \tag{15}$$

$$\overline{H}_{yz} = 2\mu \left[\left(\frac{\alpha^2}{2\beta^2} - 1 \right) \left(\frac{\partial H_{xz}}{\partial x} + \frac{\partial H_{zz}}{\partial z} \right) \right.$$
$$\left. + \frac{\alpha^2}{2\beta^2} \frac{\partial H_{yz}}{\partial y} \right] \text{(z resultant)} \tag{16}$$

In these equations, the derivatives $\frac{\partial H_{xx}}{\partial x}$, $\frac{\partial H_{xy}}{\partial x}$ and $\frac{\partial H_{xz}}{\partial x}$ are expressed by:

$$\frac{\partial H_{xx}}{\partial x} = \bar{\sigma}_{xx}^{y,x} \cos\theta + \bar{\sigma}_{yx}^{y,x} \sin\theta$$
$$\frac{\partial H_{xy}}{\partial x} = \bar{\sigma}_{yy}^{y,x} \sin\theta + \bar{\sigma}_{xy}^{y,x} \cos\theta \tag{17}$$
$$\frac{\partial H_{xz}}{\partial x} = \bar{\sigma}_{xz}^{y,x} \cos\theta + \bar{\sigma}_{yz}^{y,x} \sin\theta,$$

where $\bar{\sigma}_{xx}^{y,x} = 2\mu \left[\frac{\alpha^2}{2\beta^2} \frac{\partial^2 G_{xx}}{\partial x \partial x} + \left(\frac{\alpha^2}{2\beta^2} - 1 \right) \left(\frac{\partial^2 G_{xy}}{\partial x \partial y} + \frac{\partial^2 G_{xz}}{\partial x \partial z} \right) \right]$,

$$\bar{\sigma}_{yx}^{y,x} = \mu \left[\frac{\partial^2 G_{xy}}{\partial x \partial x} + \frac{\partial^2 G_{xx}}{\partial x \partial y} \right],$$

$$\bar{\sigma}_{yy}^{y,x} = 2\mu \left[\left(\frac{\alpha^2}{2\beta^2} - 1 \right) \left(\frac{\partial^2 G_{xx}}{\partial x \partial x} + \frac{\partial^2 G_{xz}}{\partial x \partial z} \right) + \frac{\alpha^2}{2\beta^2} \frac{\partial^2 G_{xy}}{\partial x \partial y} \right],$$

$$\bar{\sigma}_{xy}^{y,x} = \mu \left[\frac{\partial^2 G_{xy}}{\partial x \partial x} + \frac{\partial^2 G_{xx}}{\partial x \partial y} \right],$$

$$\bar{\sigma}_{xz}^{y,x} = \mu \left[\frac{\partial^2 G_{xx}}{\partial x \partial z} + \frac{\partial^2 G_{xz}}{\partial x \partial x} \right],$$

$$\bar{\sigma}_{yz}^{y,x} = \mu \left[\frac{\partial^2 G_{xy}}{\partial x \partial z} + \frac{\partial^2 G_{xz}}{\partial x \partial y} \right],$$

which can be taken as the application of a dipole load and an inertial load, defined as shown in Fig. 6.

The dynamic equilibrium of the isolated semi-cylinder, with volume V, illustrated in Fig. 6, is verified by computing the components resulting from the forces defined along the surface of the cylinder S_{sc} and from the inertial load in the volume defined by the boundary element S_{BE} and the surface of the cylinder S_{sc}:

$$\int_{S_{BE}} \frac{\partial H_{xx}}{\partial x} \mathrm{d}S_{BE} = \int_{S_{SC}} \left(\bar{\sigma}_{xx}^{y,x} \cos\theta + \bar{\sigma}_{yx}^{y,x} \sin\theta \right) \mathrm{d}S_{SC}$$
$$= \int_0^\pi \left(\bar{\sigma}_{xx}^{y,x} \cos\theta + \bar{\sigma}_{yx}^{y,x} \sin\theta \right) \frac{L}{2} \mathrm{d}\theta$$
$$= 0, \tag{18}$$

with L representing the length of the boundary element;

$$\int_{S_{BE}} \frac{\partial H_{xy}}{\partial x} \mathrm{d}S_{BE}$$
$$= \int_{S_{SC}} \left(\bar{\sigma}_{yy}^{y,x} \sin\theta + \bar{\sigma}_{xy}^{y,x} \cos\theta \right) \mathrm{d}S_{SC}$$
$$- \int_V \rho \frac{\partial \ddot{G}_{xy}}{\partial x} \mathrm{d}V$$
$$= \int_0^\pi \left(\bar{\sigma}_{yy}^{y,x} \sin\theta + \bar{\sigma}_{xy}^{y,x} \cos\theta \right) \frac{L}{2} \mathrm{d}\theta$$
$$+ \rho\omega^2 \int_0^\pi \int_0^{L/2} \frac{\partial G_{xy}}{\partial x} r \, \mathrm{d}r \, \mathrm{d}\theta$$
$$= \frac{\mathrm{i}}{2} \left[k_\alpha H_1 \left(k_\alpha \frac{L}{2} \right) \left(1 - \frac{2\beta^2}{\alpha^2} \right) \right.$$
$$\left. - \frac{4}{L k_s^2} \chi_2 (L/2) - \frac{L}{3} \frac{k_z^2}{k_s^2} \chi_2 (L/2) \right], \tag{19}$$

with $k_\beta = \sqrt{\frac{\omega^2}{\beta^2} - k_z^2}$, $k_s = \frac{\omega}{\beta}$ and $\chi_n (L/2) = k_\beta^n H_n \left(k_\beta \frac{L}{2} \right) - k_\alpha^n H_n \left(k_\alpha \frac{L}{2} \right)$;

$$\int_{S_{BE}} \frac{\partial H_{xz}}{\partial x} \mathrm{d}S_{BE} = \int_{S_{SC}} \left(\bar{\sigma}_{xz}^{y,x} \cos\theta + \bar{\sigma}_{yz}^{y,x} \sin\theta \right) \mathrm{d}S_{SC}$$
$$= \int_0^\pi \left(\bar{\sigma}_{xz}^{y,x} \cos\theta + \bar{\sigma}_{yz}^{y,x} \sin\theta \right) \frac{L}{2} \mathrm{d}\theta$$
$$= \frac{-k_z \pi L}{8k_s^2} \left[k_\beta^3 H_1 \left(k_\beta \frac{L}{2} \right) - k_\alpha^3 H_1 \left(k_\alpha \frac{L}{2} \right) \right.$$
$$\left. - \frac{1}{2} k_\beta k_s^2 H_1 \left(k_\beta \frac{L}{2} \right) \right]. \tag{20}$$

In Eqs. (14–16), $\frac{\partial H_{yx}}{\partial y}$, $\frac{\partial H_{yy}}{\partial y}$ and $\frac{\partial H_{yz}}{\partial y}$ may be defined by:

$$\frac{\partial H_{yx}}{\partial y} = \bar{\sigma}_{xx}^{y,y} \cos\theta + \bar{\sigma}_{yx}^{y,y} \sin\theta$$
$$\frac{\partial H_{yy}}{\partial y} = \bar{\sigma}_{yy}^{y,y} \sin\theta + \bar{\sigma}_{xy}^{y,y} \cos\theta \tag{21}$$
$$\frac{\partial H_{yz}}{\partial y} = \bar{\sigma}_{xz}^{y,y} \cos\theta + \bar{\sigma}_{yz}^{y,y} \sin\theta,$$

where $\bar{\sigma}_{xx}^{y,y} = 2\mu \left[\frac{\alpha^2}{2\beta^2} \frac{\partial^2 G_{yx}}{\partial y \partial x} + \left(\frac{\alpha^2}{2\beta^2} - 1 \right) \left(\frac{\partial^2 G_{yy}}{\partial y \partial y} + \frac{\partial^2 G_{yz}}{\partial y \partial z} \right) \right]$,

$$\bar{\sigma}_{yx}^{y,y} = \mu \left[\frac{\partial^2 G_{yy}}{\partial y \partial x} + \frac{\partial^2 G_{yx}}{\partial y \partial y} \right],$$

$$\bar{\sigma}_{yy}^{y,y} = 2\mu \left[\left(\frac{\alpha^2}{2\beta^2} - 1 \right) \left(\frac{\partial^2 G_{yx}}{\partial y \partial x} + \frac{\partial^2 G_{yz}}{\partial y \partial z} \right) + \frac{\alpha^2}{2\beta^2} \frac{\partial^2 G_{yy}}{\partial y \partial y} \right],$$

$$\bar{\sigma}_{xy}^{y,y} = \mu \left[\frac{\partial^2 G_{yy}}{\partial y \partial x} + \frac{\partial^2 G_{yx}}{\partial y \partial y} \right],$$

$$\bar{\sigma}_{xz}^{y,y} = \mu \left[\frac{\partial^2 G_{yx}}{\partial y \partial z} + \frac{\partial^2 G_{yz}}{\partial y \partial x} \right],$$

$$\bar{\sigma}_{yz}^{y,y} = \mu \left[\frac{\partial^2 G_{yy}}{\partial y \partial z} + \frac{\partial^2 G_{yz}}{\partial y \partial y} \right],$$

which can be understood as the result of applying a dipole load and an inertial load represented in Fig. 7.

The semi-cylinder represented in Fig. 7 corresponds to a dynamic equilibrium outlined by computing the components resulting from the forces applied along the surface of the cylinder S_{sc} and from the inertial load in the volume V defined by the boundary element S_{BE} and the surface of the cylinder S_{sc}:

$$\int_{S_{BE}} \frac{\partial H_{yx}}{\partial y} dS_{BE} = \int_{S_{SC}} \left(\bar{\sigma}_{xx}^{y,y} \cos \theta + \bar{\sigma}_{yx}^{y,y} \sin \theta \right) dS_{SC}$$

$$= \int_0^\pi \left(\bar{\sigma}_{xx}^{y,y} \cos \theta + \bar{\sigma}_{yx}^{y,y} \sin \theta \right) \frac{L}{2} d\theta = 0; \tag{22}$$

$$\int_{S_{BE}} \frac{\partial H_{yy}}{\partial y} dS_{BE}$$

$$= \int_{S_{SC}} \left(\bar{\sigma}_{yy}^{y,y} \sin \theta + \bar{\sigma}_{xy}^{y,y} \cos \theta \right) dS_{SC} - \int_V \rho \frac{\partial \ddot{G}_{yy}}{\partial y} dV$$

$$= \int_0^\pi \left(\bar{\sigma}_{yy}^{y,y} \sin \theta + \bar{\sigma}_{xy}^{y,y} \cos \theta \right) \frac{L}{2} d\theta$$

$$+ \rho \omega^2 \int_0^\pi \int_0^{L/2} \frac{\partial G_{yy}}{\partial y} r \, dr \, d\theta$$

$$= -i \left[-\frac{1}{2} k_z^2 \int_0^{L/2} H_0 (k_\beta r) \, dr - \frac{1}{2} k_\alpha^2 \int_0^{L/2} H_0 (k_\alpha r) \, dr \right.$$

$$- \frac{2}{L \, k_s^2} \chi_2 (L/2) + \frac{1}{2} k_\alpha H_1 \left(k_\alpha \frac{L}{2} \right)$$

$$+ \frac{L}{12 k_s^2} \left(-k_s^2 k_z^2 + 4 k_\alpha^4 \right) H_0 \left(k_\beta \frac{L}{2} \right)$$

$$+ \frac{k_\beta}{3} \frac{k_z^2}{k_s^2} H_1 \left(k_\beta \frac{L}{2} \right) + \frac{L}{3} \frac{k_\alpha^2 k_z^2}{k_s^2} H_0 \left(k_\alpha \frac{L}{2} \right)$$

$$\left. - \frac{k_\alpha}{3} \frac{k_z^2}{k_s^2} H_1 \left(k_\alpha \frac{L}{2} \right) \right]; \tag{23}$$

$$\int_{S_{BE}} \frac{\partial H_{yz}}{\partial y} dS_{BE} = \int_{S_{SC}} \left(\bar{\sigma}_{xz}^{y,y} \cos \theta + \bar{\sigma}_{yz}^{y,y} \sin \theta \right) dS_{SC}$$

$$= \int_0^\pi \left(\bar{\sigma}_{xz}^{y,y} \cos \theta + \bar{\sigma}_{yz}^{y,y} \sin \theta \right) \frac{L}{2} d\theta$$

$$= \frac{-k_z \pi L}{8 k_s^2} \left[k_\beta^3 H_1 \left(k_\beta \frac{L}{2} \right) - k_\alpha^3 H_1 \left(k_\alpha \frac{L}{2} \right) \right.$$

$$\left. - \frac{1}{2} k_\beta k_s^2 H_1 \left(k_\beta \frac{L}{2} \right) \right]. \tag{24}$$

In Eqs. (14–16), the derivatives in order to z, $\frac{\partial H_{zx}}{\partial z}$, $\frac{\partial H_{zy}}{\partial z}$ and $\frac{\partial H_{zz}}{\partial z}$, can be written as:

$$\frac{\partial H_{zx}}{\partial z} = \bar{\sigma}_{xx}^{y,z} \cos \theta + \bar{\sigma}_{yx}^{y,z} \sin \theta$$

$$\frac{\partial H_{zy}}{\partial z} = \bar{\sigma}_{yy}^{y,z} \sin \theta + \bar{\sigma}_{xy}^{y,z} \cos \theta \tag{25}$$

$$\frac{\partial H_{zz}}{\partial z} = \bar{\sigma}_{xz}^{y,z} \cos \theta + \bar{\sigma}_{yz}^{y,z} \sin \theta,$$

where $\bar{\sigma}_{xx}^{y,z} = 2\mu \left[\frac{\alpha^2}{2\beta^2} \frac{\partial^2 G_{zx}}{\partial z \partial x} + \left(\frac{\alpha^2}{2\beta^2} - 1 \right) \left(\frac{\partial^2 G_{zy}}{\partial z \partial y} + \frac{\partial^2 G_{zz}}{\partial z \partial z} \right) \right]$,

$$\bar{\sigma}_{yx}^{y,z} = \mu \left[\frac{\partial^2 G_{zy}}{\partial z \partial x} + \frac{\partial^2 G_{zx}}{\partial z \partial y} \right],$$

$$\bar{\sigma}_{yy}^{y,z} = 2\mu \left[\left(\frac{\alpha^2}{2\beta^2} - 1 \right) \left(\frac{\partial^2 G_{zx}}{\partial z \partial x} + \frac{\partial^2 G_{zz}}{\partial z \partial z} \right) + \frac{\alpha^2}{2\beta^2} \frac{\partial^2 G_{zy}}{\partial z \partial y} \right],$$

$$\bar{\sigma}_{xy}^{y,z} = \mu \left[\frac{\partial^2 G_{zy}}{\partial z \partial x} + \frac{\partial^2 G_{zx}}{\partial z \partial y} \right],$$

$$\bar{\sigma}_{xz}^{y,z} = \mu \left[\frac{\partial^2 G_{zx}}{\partial z \partial z} + \frac{\partial^2 G_{zz}}{\partial z \partial x} \right],$$

$$\bar{\sigma}_{yz}^{y,z} = \mu \left[\frac{\partial^2 G_{zy}}{\partial z \partial z} + \frac{\partial^2 G_{zz}}{\partial z \partial y} \right],$$

which can be seen as the application of a dipole load and an inertial load, as illustrated in Fig. 8.

The dynamic equilibrium of the detached semi-cylinder of Fig. 8 is achieved by computing the components resulting from the forces defined along the surface of the cylinder S_{sc} and from the inertial load in the volume V defined by the boundary element S_{BE} and the surface of the cylinder S_{sc}:

$$\int_{S_{BE}} \frac{\partial H_{zx}}{\partial z} dS_{BE} = \int_{S_{SC}} \left(\bar{\sigma}_{xx}^{y,z} \cos \theta + \bar{\sigma}_{yx}^{y,z} \sin \theta \right) dS_{SC}$$

$$= \int_0^\pi \left(\bar{\sigma}_{xx}^{y,z} \cos \theta + \bar{\sigma}_{yx}^{y,z} \sin \theta \right) \frac{L}{2} d\theta = 0; \tag{26}$$

$$\int\limits_{S_{BE}} \frac{\partial H_{zy}}{\partial z} dS_{BE}$$

$$= \int\limits_{S_{SC}} \left(\bar{\sigma}_{yy}^{y,z} \sin\ \theta + \bar{\sigma}_{xy}^{y,z} \cos\ \theta\right) dS_{SC} - \int\limits_{V} \rho \frac{\partial \ddot{G}_{zy}}{\partial z} dV$$

$$= \int\limits_{0}^{\pi} \left(\bar{\sigma}_{yy}^{y,z} \sin\ \theta + \bar{\sigma}_{xy}^{y,z} \cos\ \theta\right)\frac{L}{2} d\theta$$

$$+ \rho\omega^2 \int\limits_{0}^{\pi}\int\limits_{0}^{L/2} \frac{\partial G_{zy}}{\partial z} r\ dr\ d\theta$$

$$= \mathrm{i}\frac{L\,k_z^2}{4}\left[-\frac{2}{\mathrm{L}}\int\limits_0^{L/2} \mathrm{H}_0\left(k_\beta r\right)\ dr + \frac{2}{\mathrm{L}}\int\limits_0^{L/2} \mathrm{H}_0\left(k_\alpha r\right)\ dr\right.$$

$$+\frac{1}{k_p^2}\chi_2\left(L/2\right) + \left(\frac{1}{k_s^2} - \frac{1}{k_p^2}\right)\frac{4}{L}\chi_1\left(L/2\right)$$

$$-\mathrm{H}_0\left(k_\beta \frac{L}{2}\right) - \mathrm{H}_0\left(k_\alpha \frac{L}{2}\right) + \frac{k_\beta^2}{k_p^2}\mathrm{H}_0\left(k_\beta \frac{L}{2}\right)$$

$$+\frac{k_z^2}{k_p^2}\mathrm{H}_0\left(k_\alpha \frac{L}{2}\right) + 2\frac{k_z^2}{k_s^2}\mathrm{H}_0\left(k_\beta \frac{L}{2}\right)$$

$$\left.-2\frac{k_z^2}{k_s^2}\mathrm{H}_0\left(k_\alpha \frac{L}{2}\right)\right]; \tag{27}$$

$$\int\limits_{S_{BE}} \frac{\partial H_{zz}}{\partial z} dS_{BE} = \int\limits_{S_{SC}} \left(\bar{\sigma}_{xz}^{y,z} \cos\ \theta + \bar{\sigma}_{yz}^{y,z} \sin\ \theta\right) dS_{SC}$$

$$= \int\limits_0^\pi \left(\bar{\sigma}_{xz}^{y,z} \cos\ \theta + \bar{\sigma}_{yz}^{y,z} \sin\ \theta\right)\frac{L}{2} d\theta$$

$$= \frac{-k_z \pi L}{8k_s^2}\left[2k_z^2 \chi_1\left(L/2\right)\right.$$

$$\left.- k_\beta k_s^2 \mathrm{H}_1\left(k_\beta \frac{L}{2}\right)\right]. \tag{28}$$

2 Load along the tangential direction

If the load is now applied along the tangential direction, the resultants along the horizontal, vertical and z directions are obtained from Eq. (11), leading to:

$$\overline{H}_{xx} = \mu\left[\frac{\partial H_{yx}}{\partial x} + \frac{\partial H_{xx}}{\partial y}\right] \text{(horizontal resultant)} \tag{29}$$

$$\overline{H}_{xy} = \mu\left[\frac{\partial H_{yy}}{\partial x} + \frac{\partial H_{xy}}{\partial y}\right] \text{(vertical resultant)} \tag{30}$$

$$\overline{H}_{xz} = \mu\left[\frac{\partial H_{yz}}{\partial x} + \frac{\partial H_{xz}}{\partial y}\right] \text{(z resultant)} \tag{31}$$

The derivatives $\frac{\partial H_{yx}}{\partial x}$, $\frac{\partial H_{yy}}{\partial x}$ and $\frac{\partial H_{yz}}{\partial x}$ in these equations can be written as:

$$\frac{\partial H_{yx}}{\partial x} = \bar{\sigma}_{xx}^{x,x} \cos\ \theta + \bar{\sigma}_{yx}^{x,x} \sin\ \theta$$

$$\frac{\partial H_{yy}}{\partial x} = \bar{\sigma}_{yy}^{x,x} \sin\ \theta + \bar{\sigma}_{xy}^{x,x} \cos\ \theta \tag{32}$$

$$\frac{\partial H_{yz}}{\partial x} = \bar{\sigma}_{xz}^{x,x} \cos\ \theta + \bar{\sigma}_{yz}^{x,x} \sin\ \theta,$$

where $\bar{\sigma}_{xx}^{x,x} = 2\mu\left[\frac{\alpha^2}{2\beta^2}\frac{\partial^2 G_{yx}}{\partial x \partial x} + \left(\frac{\alpha^2}{2\beta^2} - 1\right)\left(\frac{\partial^2 G_{yy}}{\partial x \partial y} + \frac{\partial^2 G_{yz}}{\partial x \partial z}\right)\right]$,

$$\bar{\sigma}_{yx}^{x,x} = \mu\left[\frac{\partial^2 G_{yy}}{\partial x \partial x} + \frac{\partial^2 G_{yx}}{\partial x \partial y}\right],$$

$$\bar{\sigma}_{yy}^{x,x} = 2\mu\left[\left(\frac{\alpha^2}{2\beta^2} - 1\right)\left(\frac{\partial^2 G_{yx}}{\partial x \partial x} + \frac{\partial^2 G_{yz}}{\partial x \partial z}\right)\right.$$
$$\left.+ \frac{\alpha^2}{2\beta^2}\frac{\partial^2 G_{yy}}{\partial x \partial y}\right],$$

$$\bar{\sigma}_{xy}^{x,x} = \mu\left[\frac{\partial^2 G_{yy}}{\partial x \partial x} + \frac{\partial^2 G_{yx}}{\partial x \partial y}\right],$$

$$\bar{\sigma}_{xz}^{x,x} = \mu\left[\frac{\partial^2 G_{yx}}{\partial x \partial z} + \frac{\partial^2 G_{yz}}{\partial x \partial x}\right],$$

$$\bar{\sigma}_{yz}^{x,x} = \mu\left[\frac{\partial^2 G_{yy}}{\partial x \partial z} + \frac{\partial^2 G_{yz}}{\partial x \partial y}\right].$$

This procedure can be interpreted as the application of a dipole load and an inertial load, as defined schematically in Fig. 9.

Considering the dynamic equilibrium of the semi-cylinder given in Fig. 9, which is defined by the computation of the components resulting from the forces defined along the surface of the cylinder S_{sc} and from the inertial load in the volume V, formed by the boundary element S_{BE} and the surface of the cylinder S_{sc}, the following integrals are evaluated:

$$\int\limits_{S_{BE}} \frac{\partial H_{yx}}{\partial x} dS_{BE}$$

$$= \int\limits_{S_{SC}} \left(\bar{\sigma}_{xx}^{x,x} \cos\ \theta + \bar{\sigma}_{yx}^{x,x} \sin\ \theta\right) dS_{SC} - \int\limits_{V} \rho \frac{\partial \ddot{G}_{yx}}{\partial x} dV$$

$$= \int\limits_0^\pi \left(\bar{\sigma}_{xx}^{x,x} \cos\ \theta + \bar{\sigma}_{yx}^{x,x} \sin\ \theta\right)\frac{L}{2} d\theta$$

$$+ \rho\omega^2 \int\limits_0^\pi\int\limits_0^{L/2} \frac{\partial G_{yx}}{\partial x} r\ dr\ d\theta$$

$$= \frac{\mathrm{i}}{2}\left[k_\beta \mathrm{H}_1\left(k_\beta \frac{L}{2}\right) - \frac{4}{L\,k_s^2}\chi_2\left(L/2\right) - \frac{L}{3}\frac{k_z^2}{k_s^2}\chi_2\left(L/2\right)\right]; \tag{33}$$

$$\int\limits_{S_{BE}} \frac{\partial H_{yy}}{\partial x} dS_{BE} = \int\limits_{S_{SC}} \left(\bar{\sigma}_{yy}^{x,x} \sin\ \theta + \bar{\sigma}_{xy}^{x,x} \cos\ \theta\right) dS_{SC}$$

$$= \int\limits_0^\pi \left(\bar{\sigma}_{yy}^{x,x} \sin\ \theta + \bar{\sigma}_{xy}^{x,x} \cos\ \theta\right)\frac{L}{2} d\theta = 0; \tag{34}$$

$$\int\limits_{S_{BE}} \frac{\partial H_{yz}}{\partial x} \mathrm{d}S_{BE} = \int\limits_{S_{SC}} \left(\bar{\sigma}_{xz}^{x,x} \cos\ \theta + \bar{\sigma}_{yz}^{x,x} \sin\ \theta \right) \mathrm{d}S_{SC}$$

$$= \int\limits_{0}^{\pi} \left(\bar{\sigma}_{xz}^{x,x} \cos\ \theta + \bar{\sigma}_{yz}^{x,x} \sin\ \theta \right) \frac{L}{2} \mathrm{d}\theta = 0.$$

$$(35)$$

The derivatives in order to y in Eqs. (29–31), represented by $\frac{\partial H_{xx}}{\partial y}$, $\frac{\partial H_{xy}}{\partial y}$ and $\frac{\partial H_{xz}}{\partial y}$, can be formulated by:

$$\frac{\partial H_{xx}}{\partial y} = \bar{\sigma}_{xx}^{x,y} \cos\ \theta + \bar{\sigma}_{yx}^{x,y} \sin\ \theta$$

$$\frac{\partial H_{xy}}{\partial y} = \bar{\sigma}_{yy}^{x,y} \sin\ \theta + \bar{\sigma}_{xy}^{x,y} \cos\ \theta \qquad (36)$$

$$\frac{\partial H_{xz}}{\partial y} = \bar{\sigma}_{xz}^{x,y} \cos\ \theta + \bar{\sigma}_{yz}^{x,y} \sin\ \theta,$$

where $\bar{\sigma}_{xx}^{x,y} = 2\mu \left[\frac{\alpha^2}{2\beta^2} \frac{\partial^2 G_{xx}}{\partial y \partial x} + \left(\frac{\alpha^2}{2\beta^2} - 1 \right) \left(\frac{\partial^2 G_{xy}}{\partial y \partial y} + \frac{\partial^2 G_{xz}}{\partial y \partial z} \right) \right]$,

$$\bar{\sigma}_{yx}^{x,y} = \mu \left[\frac{\partial^2 G_{yy}}{\partial y \partial x} + \frac{\partial^2 G_{xx}}{\partial y \partial y} \right],$$

$$\bar{\sigma}_{yy}^{x,y} = 2\mu \left[\left(\frac{\alpha^2}{2\beta^2} - 1 \right) \left(\frac{\partial^2 G_{xx}}{\partial y \partial x} + \frac{\partial^2 G_{xz}}{\partial y \partial z} \right) + \frac{\alpha^2}{2\beta^2} \frac{\partial^2 G_{xy}}{\partial y \partial y} \right],$$

$$\bar{\sigma}_{xy}^{x,y} = \mu \left[\frac{\partial^2 G_{xy}}{\partial y \partial x} + \frac{\partial^2 G_{xx}}{\partial y \partial y} \right],$$

$$\bar{\sigma}_{xz}^{x,y} = \mu \left[\frac{\partial^2 G_{xx}}{\partial y \partial z} + \frac{\partial^2 G_{xz}}{\partial y \partial x} \right],$$

$$\bar{\sigma}_{yz}^{x,y} = \mu \left[\frac{\partial^2 G_{xy}}{\partial y \partial z} + \frac{\partial^2 G_{xz}}{\partial y \partial y} \right],$$

which can be illustrated as in Fig. 10, as the application of a dipole load and an inertial load.

The dynamic equilibrium of the semi-cylinder represented in Fig. 10 is formulated by computing the components resulting from the forces actuating along the surface of the cylinder S_{sc} and from the inertial load in the volume V, delimited by the boundary element S_{BE} and by the upper surface of the

cylinder S_{sc}:

$$\int\limits_{S_{BE}} \frac{\partial H_{xx}}{\partial y} \mathrm{d}S_{BE}$$

$$= \int\limits_{S_{SC}} \left(\bar{\sigma}_{xx}^{x,y} \cos\ \theta + \bar{\sigma}_{yx}^{x,y} \sin\ \theta \right) \mathrm{d}S_{SC} - \int\limits_{V} \rho \frac{\partial \ddot{G}_{xx}}{\partial y} \mathrm{d}V$$

$$= \int\limits_{0}^{\pi} \left(\bar{\sigma}_{xx}^{x,y} \cos\ \theta + \bar{\sigma}_{yx}^{x,y} \sin\ \theta \right) \frac{L}{2} \mathrm{d}\theta$$

$$+ \rho\omega^2 \int\limits_{0}^{\pi} \int\limits_{0}^{L/2} \frac{\partial G_{xx}}{\partial y} r\ \mathrm{d}r\ \mathrm{d}\theta$$

$$= \frac{\mathrm{i}}{2} \left[k_s^2 \int\limits_{0}^{L/2} \mathrm{H}_0 \left(k_\beta r \right) \mathrm{d}r - \left(\frac{4}{L} + \frac{L\,k_z^2}{3} \right) \frac{1}{k_s^2} \chi_2 \left(L/2 \right) \right.$$

$$\left. - k_\beta \mathrm{H}_1 \left(k_\beta \frac{L}{2} \right) - \frac{L}{2} \left(k_s^2 - k_\beta^2 \right) \mathrm{H}_0 \left(k_\beta \frac{L}{2} \right) \right];$$

$$(37)$$

$$\int\limits_{S_{BE}} \frac{\partial H_{xy}}{\partial y} \mathrm{d}S_{BE} = \int\limits_{S_{SC}} \left(\bar{\sigma}_{yy}^{x,y} \sin\ \theta + \bar{\sigma}_{xy}^{x,y} \cos\ \theta \right) \mathrm{d}S_{SC}$$

$$= \int\limits_{0}^{\pi} \left(\bar{\sigma}_{yy}^{x,y} \sin\ \theta + \bar{\sigma}_{xy}^{x,y} \cos\ \theta \right) \frac{L}{2} \mathrm{d}\theta = 0;$$

$$(38)$$

$$\int\limits_{S_{BE}} \frac{\partial H_{xz}}{\partial y} \mathrm{d}S_{BE} = \int\limits_{S_{SC}} \left(\bar{\sigma}_{xz}^{x,y} \cos\ \theta + \bar{\sigma}_{yz}^{x,y} \sin\ \theta \right) \mathrm{d}S_{SC}$$

$$= \int\limits_{0}^{\pi} \left(\bar{\sigma}_{xz}^{x,y} \cos\ \theta + \bar{\sigma}_{yz}^{x,y} \sin\ \theta \right) \frac{L}{2} \mathrm{d}\theta = 0.$$

$$(39)$$

3 Load along the z direction

When the load is applied along the z direction, the resultants along the 3 directions (horizontal, vertical and z) are given by:

$$\overline{H}_{zx} = \mu \left[\frac{\partial H_{yx}}{\partial z} + \frac{\partial H_{zx}}{\partial y} \right] \text{ (horizontal resultant)} \qquad (40)$$

$$\overline{H}_{zy} = \mu \left[\frac{\partial H_{yy}}{\partial z} + \frac{\partial H_{zy}}{\partial y} \right] \text{ (vertical resultant)} \qquad (41)$$

$$\overline{H}_{zz} = \mu \left[\frac{\partial H_{yz}}{\partial z} + \frac{\partial H_{zz}}{\partial y} \right] \text{ (z resultant)} \qquad (42)$$

In these equations, the derivatives $(\frac{\partial H_{yx}}{\partial z}, \frac{\partial H_{yy}}{\partial z}$ and $\frac{\partial H_{yz}}{\partial z})$ in the z direction are defined as follows:

$$\frac{\partial H_{yx}}{\partial z} = \bar{\sigma}_{xx}^{z,z} \cos\,\theta + \bar{\sigma}_{yx}^{z,z} \sin\,\theta$$

$$\frac{\partial H_{yy}}{\partial z} = \bar{\sigma}_{yy}^{z,z} \sin\,\theta + \bar{\sigma}_{xy}^{z,z} \cos\,\theta \qquad (43)$$

$$\frac{\partial H_{yz}}{\partial z} = \bar{\sigma}_{xz}^{z,z} \cos\,\theta + \bar{\sigma}_{yz}^{z,z} \sin\,\theta,$$

where $\bar{\sigma}_{xx}^{z,z} = 2\mu \left[\frac{\alpha^2}{2\beta^2} \frac{\partial^2 G_{yx}}{\partial z \partial x} + \left(\frac{\alpha^2}{2\beta^2} - 1 \right) \left(\frac{\partial^2 G_{yy}}{\partial z \partial y} + \frac{\partial^2 G_{yz}}{\partial z \partial z} \right) \right]$,

$$\bar{\sigma}_{yx}^{z,z} = \mu \left[\frac{\partial^2 G_{yy}}{\partial z \partial x} + \frac{\partial^2 G_{yx}}{\partial z \partial y} \right],$$

$$\bar{\sigma}_{yy}^{z,z} = 2\mu \left[\left(\frac{\alpha^2}{2\beta^2} - 1 \right) \left(\frac{\partial^2 G_{yx}}{\partial z \partial x} + \frac{\partial^2 G_{yz}}{\partial z \partial z} \right) \right.$$
$$\left. + \frac{\alpha^2}{2\beta^2} \frac{\partial^2 G_{yy}}{\partial z \partial y} \right],$$

$$\bar{\sigma}_{xy}^{z,z} = \mu \left[\frac{\partial^2 G_{yy}}{\partial z \partial x} + \frac{\partial^2 G_{yx}}{\partial z \partial y} \right],$$

$$\bar{\sigma}_{xz}^{z,z} = \mu \left[\frac{\partial^2 G_{yx}}{\partial z \partial z} + \frac{\partial^2 G_{yz}}{\partial z \partial x} \right],$$

$$\bar{\sigma}_{yz}^{z,z} = \mu \left[\frac{\partial^2 G_{yy}}{\partial z \partial z} + \frac{\partial^2 G_{yz}}{\partial z \partial y} \right],$$

which can be interpreted as the application of a dipole load and an inertial load, as defined in Fig. 11.

The dynamic equilibrium of this semi-cylinder of volume V (see Fig. 11) is formulated by determining the components resulting from the forces applied along the surface of the cylinder S_{sc} and from the inertial load acting in the body defined by the boundary element S_{BE} and the surface of the cylinder S_{sc}:

$$\int_{S_{BE}} \frac{\partial H_{yx}}{\partial z} dS_{BE} = \int_{S_{SC}} (\bar{\sigma}_{xx}^{z,z} \cos\,\theta + \bar{\sigma}_{yx}^{z,z} \sin\,\theta) dS_{SC}$$
$$= \int_0^\pi (\bar{\sigma}_{xx}^{z,z} \cos\,\theta + \bar{\sigma}_{yx}^{z,z} \sin\,\theta) \frac{L}{2} d\theta = 0; \qquad (44)$$

$$\int_{S_{BE}} \frac{\partial H_{yy}}{\partial z} dS_{BE}$$
$$= \int_{S_{SC}} (\bar{\sigma}_{yy}^{z,z} \sin\,\theta + \bar{\sigma}_{xy}^{z,z} \cos\,\theta) dS_{SC}$$
$$= \int_0^\pi (\bar{\sigma}_{yy}^{z,z} \sin\,\theta + \bar{\sigma}_{xy}^{z,z} \cos\,\theta) \frac{L}{2} d\theta$$
$$= \frac{-k_z \pi L}{8 k_s^2} \left[-k_z^2 \chi_1 (L/2) - \frac{1}{2} k_s^2 k_\beta H_1 \left(k_\beta \frac{L}{2} \right) \right.$$
$$\left. - \frac{1}{2} k_s^2 k_\alpha H_1 \left(k_\alpha \frac{L}{2} \right) \right]; \qquad (45)$$

$$\int_{S_{BE}} \frac{\partial H_{yz}}{\partial z} dS_{BE}$$
$$= \int_{S_{SC}} (\bar{\sigma}_{xz}^{z,z} \cos\,\theta + \bar{\sigma}_{yz}^{z,z} \sin\,\theta) dS_{SC} - \int_V \rho \frac{\partial \ddot{G}_{yz}}{\partial z} dV$$
$$= \int_0^\pi (\bar{\sigma}_{xz}^{z,z} \cos\,\theta + \bar{\sigma}_{yz}^{z,z} \sin\,\theta) \frac{L}{2} d\theta$$
$$+ \rho \omega^2 \int_0^\pi \int_0^{L/2} \frac{\partial G_{yz}}{\partial z} r\, dr\, d\theta$$
$$= -\frac{i k_z^2}{2} \left[\int_0^{L/2} H_0 (k_\beta r)\, dr - \int_0^{L/2} H_0 (k_\alpha r)\, dr - \frac{L}{k_s^2} \chi_2 (L/2) \right.$$
$$+ \frac{2}{k_s^2} \chi_1 (L/2) - L\, H_0 \left(k_\beta \frac{L}{2} \right)$$
$$\left. + \frac{L}{2} H_0 \left(k_\alpha \frac{L}{2} \right) \right]. \qquad (46)$$

The definition of the derivatives $\frac{\partial H_{zx}}{\partial y}, \frac{\partial H_{zy}}{\partial y}$ and $\frac{\partial H_{zz}}{\partial y}$, in Eqs. (40–42), is given by:

$$\frac{\partial H_{zx}}{\partial y} = \bar{\sigma}_{xx}^{z,y} \cos\,\theta + \bar{\sigma}_{yx}^{z,y} \sin\,\theta$$

$$\frac{\partial H_{zy}}{\partial y} = \bar{\sigma}_{yy}^{z,y} \sin\,\theta + \bar{\sigma}_{xy}^{z,y} \cos\,\theta \qquad (47)$$

$$\frac{\partial H_{zz}}{\partial y} = \bar{\sigma}_{xz}^{z,y} \cos\,\theta + \bar{\sigma}_{yz}^{z,y} \sin\,\theta,$$

where $\bar{\sigma}_{xx}^{z,y} = 2\mu \left[\frac{\alpha^2}{2\beta^2} \frac{\partial^2 G_{zx}}{\partial y \partial x} + \left(\frac{\alpha^2}{2\beta^2} - 1 \right) \left(\frac{\partial^2 G_{zy}}{\partial y \partial y} + \frac{\partial^2 G_{zz}}{\partial y \partial z} \right) \right]$,

$$\bar{\sigma}_{yx}^{z,y} = \mu \left[\frac{\partial^2 G_{zy}}{\partial y \partial x} + \frac{\partial^2 G_{zx}}{\partial y \partial y} \right],$$

$$\bar{\sigma}_{yy}^{z,y} = 2\mu \left[\left(\frac{\alpha^2}{2\beta^2} - 1 \right) \left(\frac{\partial^2 G_{zx}}{\partial y \partial x} + \frac{\partial^2 G_{zz}}{\partial y \partial z} \right) \right.$$
$$\left. + \frac{\alpha^2}{2\beta^2} \frac{\partial^2 G_{zy}}{\partial y \partial y} \right],$$

$$\bar{\sigma}_{xy}^{z,y} = \mu \left[\frac{\partial^2 G_{zy}}{\partial y \partial x} + \frac{\partial^2 G_{zx}}{\partial y \partial y} \right],$$

$$\bar{\sigma}_{xz}^{z,y} = \mu \left[\frac{\partial^2 G_{zx}}{\partial y \partial z} + \frac{\partial^2 G_{zz}}{\partial y \partial x} \right],$$

$$\bar{\sigma}_{yz}^{z,y} = \mu \left[\frac{\partial^2 G_{zy}}{\partial y \partial z} + \frac{\partial^2 G_{zz}}{\partial y \partial y} \right],$$

and this can now be seen as the application of a dipole load and an inertial load, defined as shown in Fig. 12.

Performing the dynamic equilibrium of the semi-cylinder in Fig. 12 by calculating the components resulting from the forces acting along the surface of the cylinder S_{sc} and from the inertial load applied in the volume V, defined

by the boundary element S_{BE} and the surface of the cylinder S_{sc}, leads to these integrals:

$$\int_{S_{BE}} \frac{\partial H_{zx}}{\partial y} dS_{BE} = \int_{S_{SC}} \left(\bar{\sigma}_{xx}^{z,y} \cos\theta + \bar{\sigma}_{yx}^{z,y} \sin\theta \right) dS_{SC}$$

$$= \int_0^\pi \left(\bar{\sigma}_{xx}^{z,y} \cos\theta + \bar{\sigma}_{yx}^{z,y} \sin\theta \right) \frac{L}{2} d\theta = 0; \tag{48}$$

$$\int_{S_{BE}} \frac{\partial H_{zy}}{\partial y} dS_{BE}$$

$$= \int_{S_{SC}} \left(\bar{\sigma}_{yy}^{z,y} \sin\theta + \bar{\sigma}_{xy}^{z,y} \cos\theta \right) dS_{SC}$$

$$= \int_0^\pi \left(\bar{\sigma}_{yy}^{z,y} \sin\theta + \bar{\sigma}_{xy}^{z,y} \cos\theta \right) \frac{L}{2} d\theta$$

$$= \frac{-k_z \pi L}{8 k_s^2} \left[-k_z^2 \chi_1 (L/2) + \frac{1}{2} k_s^2 \chi_1 (L/2) \right. $$
$$\left. + \frac{1}{2} k_s^2 k_\beta H_1 \left(k_\beta \frac{L}{2} \right) \right]; \tag{49}$$

$$\int_{S_{BE}} \frac{\partial H_{zz}}{\partial y} dS_{BE}$$

$$= \int_{S_{SC}} \left(\bar{\sigma}_{xz}^{z,y} \cos\theta + \bar{\sigma}_{yz}^{z,y} \sin\theta \right) dS_{SC} - \int_V \rho \frac{\partial \ddot{G}_{zz}}{\partial z} dV$$

$$= \int_0^\pi \left(\bar{\sigma}_{xz}^{z,y} \cos\theta + \bar{\sigma}_{yz}^{z,y} \sin\theta \right) \frac{L}{2} d\theta$$

$$+ \rho \omega^2 \int_0^\pi \int_0^{L/2} \frac{\partial G_{zz}}{\partial z} r \, dr \, d\theta$$

$$= \frac{i L}{2} \left[\frac{k_\beta^2}{L} \int_0^{L/2} H_0 (k_\beta r) \, dr + \frac{k_z^2}{L} \int_0^{L/2} H_0 (k_\alpha r) \, dr \right.$$

$$+ \frac{k_z^2}{k_s^2} \chi_2 (L/2) - \frac{2 k_z^2}{L k_s^2} \chi_1 (L/2) - \frac{k_\beta^2}{2} H_2 \left(k_\beta \frac{L}{2} \right)$$

$$+ \frac{k_\beta}{L} H_1 \left(k_\beta \frac{L}{2} \right) - \frac{k_\beta^2}{2} H_0 \left(k_\beta \frac{L}{2} \right)$$

$$\left. - \frac{k_z^2}{2} H_0 \left(k_\alpha \frac{L}{2} \right) \right]. \tag{50}$$

References

1. Aliabadi MH (1997) Boundary element methods formulations in fracture mechanics. Appl Mech Rev 50:93–96
2. Aliabadi MH (1997) A new generation of boundary element methods in fracture mechanics. Int J Fracture 86:91–125
3. António J, Tadeu A (2002) 3D Seismic response of a limited valley via BEM using 2.5D analytical Green's functions for an infinite free-rigid layer. J Soil Dyn Earthquake Eng 22:659–673
4. Bouchon M, Aki K (1977) Discrete wave-number representation of seismic-source wave field. Bull Seism Soc Am 67:259–277
5. Budreck DE, Achenbach JD (1988) Scattering from three-dimensional planar cracks by the boundary integral equation method. J Appl Mech 55:405–412
6. Burton AJ, Miller GF (1971) The application of the integral equation method to the numerical solution of some exterior boundary value problems. Proc R Soc London Ser A 323:201–210
7. Chien CC, Rajiyah H, Atluri SN (1990) An effective method for solving the hypersingular integral equations in 3D acoustics. J Acoustic Soc Am 88(2):918–937
8. Cruse TA (1987) Boundary Element Analysis in Computational Fracture Mechanics. Kluwer Academic Publishers
9. Cruse TA, Richardson JD (1996) Nonsingular Somigliana stress identities in elasticity. Int J Numer Meth Eng 39:3273–3304
10. Dell'erba DN, Aliabadi MH, Rooke DP (1998) Dual boundary element method for three-dimensional thermoelastic crack problems. Int J Fracture 94:89–101
11. Dominguez J, Gallego R (1992) Time domain boundary element method for dynamic stress intensity factor computations. Int J Numer Meth Eng 33:635–647
12. Dominguez J, Ariza MP, Gallego R (2000) Flux and traction boundary elements without hypersingular or strongly singular integrals. Int J Numer Meth Eng 48:111–135
13. Fedelinski P, Aliabadi MH, Rooke DP (1994) The dual boundary element method: $\hat{J}$−integral for dynamic stress intensity factors. Int J Fracture 65(4):369–381
14. Fedelinski P, Aliabadi MH, Rooke DP (1995) A sinlge-region time domain BEM for dynamic crack problems. Int J Solids Struct 32:3555–3571
15. Fedelinski P, Aliabadi MH, Rooke DP (1996) The Laplace transform DBEM for mixed-mode dynamic crack analysis. Comp Struct 59:1021–1031
16. Fedelinski P, Aliabadi MH, Rooke DP (1996) Boundary element formulations for the dynamic analysis of cracked structures. EABE – Eng Anal Bound Elem 17:45–56
17. Guiggiani M (1998) Formulation and numerical treatment of boundary integral equations with hypersingular kernels. Singular Integrals in Boundary Element Methods, Computational Mechanics Publications, Southampton (UK) & Boston (USA)
18. Kausel E, Roesset JM (1992) Frequency domain analysis of undamped systems. J Eng Mech ASCE 118(4):721–734
19. Lutz E, Ingraffea AR, Gray LJ (1992) Use of 'simple solutions' for boundary integral methods in elasticity and fracture analysis. Int J Numer Meth Eng 35:1737–1751
20. Manolis GD, Beskos DE (1988) Boundary Element Methods in Elastodynamics. Unwin Hyman (sold to Chapman and Hall), London
21. Mi Y, Aliabadi MH (1992) Dual boundary element method for three-dimensional fracture mechanics analysis. EABE – Eng Anal Bound Elem 10:161–171
22. Pao YH, Mow CC (1973) Diffraction of Elastic Waves and Dynamic Stress Concentrations. Crane and Russak
23. Partridge PE, Brebbia CA, Wrobel LC (1992) The Dual Reciprocity Boundary Element Methods. CMP, Southampton
24. Portela A, Aliabadi MH, Rooke DP (1992) The dual boundary element method: effective implementation for crack problems. Int J Numer Meth Eng 33:1269–1287
25. Prosper D, Kausel E (2001) Wave scattering by cracks in laminated media. In: Atluri SN, Nishioka T, Kikuchi M (eds), CD: Advances in Computational Engineering and Sciences. Proceedings of the international Conference on Computational Engineering and Science ICES'01, Puerto Vallarta, Mexico,19-25/08/2001. Tech Science Press
26. Prosper D (2001) Modeling and Detection of Delaminations in Laminated Plates. PhD Thesis, MIT, Cambridge

27. Pyl L, Clouteau D, Degrande G (2004) A weakly singular boundary integral equation inelastodynamics for heterogeneous domains mitigating ficticious eigenfrequencies. EABE – Eng Anal Bound Elem 28(12):1493–1513
28. Qian ZY, Han ZD, Ufimtsev P, Atluri SN (2004) Non-hyper-singular boundary integral equations for acoustic problems, implemented by the collocation-based boundary element method. CMES – Comput Model Eng 6(2):133–144
29. Rudolphi TJ (1991) The use of simple solutions in the regularisation of hypersingular boundary integral equations. Math Comp Model 15:269–278
30. Sladek V, Sladek J (1984) Transient elastodynamic three-dimensional problems in cracked bodies. Appl Math Model 8:2–10
31. Sládek V, Sládek J (1987) A boundary integral equation method for dynamic crack problems. Eng Fracture Mech 27(3):269–277
32. Sladek V, Sladek J, Tanaka M (1992) Numerical solution of nonsingular BIE for crack problems. In: Brebbia CA, Domínguez J, Paris F (eds) Boundary Elements XIV. vol. 2, Computational Mechanics Publications, Southampton
33. Sladek J, Sladek V (2000) Nonsingular traction BIEs for crack problems in elastodynamics. Comput Mech 25:590–599
34. Stamos AA, Beskos DE (1996) 3-D seismic response analysis of long lined tunnels in half-space. J Soil Dyn Earthquake Eng 15:111–118
35. Tadeu AJB (1992) Modelling and Seismic Imaging of Buried Structures. PhD Thesis, MIT, Cambridge
36. Tadeu A, Santos P, Kausel E (1999) Closed-form Integration of Singular Terms for Constant, Linear and Quadratic Boundary Elements - Part I: SH Wave Propagation. EABE – Eng Anal Bound Elem 23(8):671–681
37. Tadeu A, Santos P, Kausel E (1999) Closed-form Integration of Singular Terms for Constant, Linear and Quadratic Boundary Elements - Part II: SV-P Wave Propagation. EABE – Eng Anal Bound Elem 23(9):757–768
38. Tadeu A, Kausel E (2000) Green's Functions for Two-and-a-half Dimensional Elastodynamic Problems. J Eng Mech, ASCE 126(10):1093–1097
39. Tadeu A, Godinho L, Santos P (2001) Performance of the BEM solution in 3D acoustic wave scattering. J Adv Eng Software 32:629–639
40. Tadeu A, António J, Kausel E (2002) 3D Scattering of waves by a cylindrical irregular cavity of infinite length in a homogeneous elastic medium. Comp Method Appl Mech Eng 191(27–28): 3015–3033
41. Takakuda K (1983) Diffraction of plane harmonic waves by cracks. JSME 26(214): 487–493
42. Tanaka M, Sladek V, Sladek J (1994) Regularization techniques applied to boundary element methods. Appl Mech Rev 47:457–499
43. Watson JO (1995) Singular boundary elements for the analysis of cracks in plane strain. Int J Numer Meth Eng 38:2389–2411
44. Wu TW, Seybert AF, Wan GC (1991) On the numerical implementation of a Cauchy principal value integral to insure a unique solution for acoustic radiation and scattering. J Acoust Soc Am 90:554–560
45. Yan ZY, Hung KC, Zheng H (2003) Solving the hypersingular boundary integral equation in three-dimensional acoustics using a regularization relationship. J Acoust Soc Am 113(5):2674–2683
46. Young A (1992) A single-domain boundary element method for 3-D elastostatic crack analysis using continuous elements. Int J Numer Meth Eng 39:1265–1293